STUDY ON NON STANDARD INTERACTION OF NEUTRINO AND UNPARTICLE PHYSICS WITH NEUTRINO-ELECTRON SCATTERING DATA AT LOW ENERGY IN TEXONO EXPERIMENT

A THESIS SUBMITTED TO
THE GRADUATE SCHOOL OF NATURAL AND APPLIED SCIENCES
OF
MIDDLE EAST TECHNICAL UNIVERSITY

BY

SELÇUK BİLMİŞ

IN PARTIAL FULFILLMENT OF THE REQUIREMENTS
FOR
THE DEGREE OF MASTER OF SCIENCE
IN
PHYSICS

SEPTEMBER 2010

Approval of the thesis:

STUDY ON NON STANDARD INTERACTION OF NEUTRINO AND UNPARTICLE PHYSICS WITH NEUTRINO-ELECTRON SCATTERING DATA AT LOW ENERGY IN TEXONO EXPERIMENT

submitted by **SELÇUK BİLMİŞ** in partial fulfillment of the requirements for the degree of **Master of Science in Physics Department, Middle East Technical University** by,

Prof. Dr. Canan Özgen _____
Dean, Graduate School of **Natural and Applied Sciences**

Prof. Dr. Sinan Bilikmen _____
Head of Department, **Physics**

Prof. Dr. Mehmet Zeyrek _____
Supervisor, **Physics Department, METU**

Dr. Muhammed Deniz _____
Co-supervisor, **ACADEMIA SINICA**

Examining Committee Members:

Prof. Dr. Ali Ulvi Yılmazer
Physics Department, Ankara University _____

Prof. Dr. Mehmet Zeyrek
Physics Department, METU _____

Assoc. Prof. Dr. Altuğ Özpineci
Physics Department, METU _____

Prof. Dr. Meltem Serin
Physics Department, METU _____

Prof. Dr. Takhmasib M. Aliev
Physics Department, METU _____

Date: _____

I hereby declare that all information in this document has been obtained and presented in accordance with academic rules and ethical conduct. I also declare that, as required by these rules and conduct, I have fully cited and referenced all material and results that are not original to this work.

Name, Last Name: SELÇUK BİLMİŞ

Signature :

ABSTRACT

STUDY ON NON STANDARD INTERACTION OF NEUTRINO AND UNPARTICLE PHYSICS WITH NEUTRINO-ELECTRON SCATTERING DATA AT LOW ENERGY IN TEXONO EXPERIMENT

Bilmiş, Selçuk
M.Sc, Department of Physics
Supervisor : Prof. Dr. Mehmet Zeyrek
Co-Supervisor : Dr. Muhammed Deniz

September 2010, 70 pages

Neutrino-electron scatterings are purely leptonic processes with robust Standard Model (SM) predictions. Their measurements can therefore provide constraints to physics beyond SM. The $\bar{\nu}_e - e^-$ data taken at the Kuo-Sheng Reactor Neutrino Laboratory were used to probe two sceneria: Non-Standard Neutrino Interactions (NSI) and Unparticle Physics. New constraints were placed to the NSI parameters (ε_{ee}^{eL}, ε_{ee}^{eR}), ($\varepsilon_{e\mu}^{eL}$, $\varepsilon_{e\mu}^{eR}$) and ($\varepsilon_{e\tau}^{eL}$, $\varepsilon_{e\tau}^{eR}$) , as well as to the coupling constants for scalar (λ_0) and vector (λ_1) unparticles to the neutrinos and electrons.

Keywords: Non-Standard Interaction, Unparticle, Texono, Neutrino Electron Scattering, Neutrino

ÖZ

TEXONO DENEYİNDE DÜŞÜK ENERJİDE NÖTRİNO-ELEKTRON SAÇILIMINDAN STANDARD OLMAYAN NÖTRİNO ETKİLEŞİMLERİ VE UNPARTİCLE FİZİK ÇALIŞILMASI

Bilmiş, Selçuk
Yüksek Lisans, Fizik Bölümü
Tez Yöneticisi : Prof. Dr. Mehmet Zeyrek
Ortak Tez Yöneticisi : Dr. Muhammed Deniz

Eylül 2010, 70 sayfa

Nötrino elektron saçılımları Standard Modelle çok iyi açıklanan leptonik etkileşmelerdir. Bu yüzden nötrino-elektron saçılımı ölçümleri, Standart Model ötesi fiziğe sınır koyabilmeyi sağlar. Kuo-Sheng Reaktör Nötrino Labaratuvarında alınan $\bar{\nu}_e - e^-$ saçılım datası iki senaryo araştırmasında kullanıldı: Nötrinoların Standart olmayan etkileşimleri ve Unparticle fiziği. Skaler (λ_0) ve vektör (λ_1) Unparticle'ın nötrino ve elektrona bağlanma sabitleriyle birlikte Standart olmayan etkileşim parametrelerine (ε_{ee}^{eL}, ε_{ee}^{eR}), ($\varepsilon_{e\mu}^{eL}$, $\varepsilon_{e\mu}^{eR}$) and ($\varepsilon_{e\tau}^{eL}$, $\varepsilon_{e\tau}^{eR}$) sınır koyuldu.

Anahtar Kelimeler: Standard Olmayan Etkileşim, Unparticle, Texono, Nötrino Elektron Saçılımı,Nötrino

To my family and passed away cat, Pisuna

ACKNOWLEDGMENTS

I wish to thank first and foremost to Prof. Dr. Henry Tsz-King Wong for giving me the opportunity of working in TEXONO Experiment in Academia Sinica.

I would like to thank my supervisor, Prof. Dr. Mehmet Zeyrek, for his guidance as well as the support he has given me ever since I was an undergraduate student. It was with his encouragements that I chose to study in this program.

I owe my deepest gratitude to my cosupervisor, Dr. Muhammed Deniz, for persuading me to study in the TEXONO Experiment. His perceptiveness, encouragement, patience and friendship played a crucial role in conclusion of this study. I am also thankful to his guidance for living in Taiwan.

I would like to thank all members of the TEXONO, for their being helpful and for making my life enjoyable in Taiwan.

Also, I want to thank to my friends, Deniz Olgu Devecioğlu, Halil Gamsızkan, Mete Kurşun, Murat Mesta, Rıfat Öcal, Serkan Kır, Sinan Değer and Uğur Emrah Surat for their friendship and support in this work. I am also thankful to Imameddin Amiraslan, Famil Veliyev , Riyayet Ismailof, Abdil Özdemir and Ozan Yıldırım for their companionship and for making my life colorful in Taiwan.

I am indebted to my family for their encouragement and great support during my thesis study.

I would like to thank to Scientific and Technological Research Council of Turkey (TUBITAK) for partial financial support during this study.

TABLE OF CONTENTS

ABSTRACT iv

ÖZ v

ACKNOWLEDGMENTS vii

TABLE OF CONTENTS viii

LIST OF TABLES x

LIST OF FIGURES xi

CHAPTERS

1 INTRODUCTION 1

1.1 β Decay Anomaly 3

1.1.1 Spin Statistics problem of β Decay 6

1.1.1.1 The Idea of Neutrino 7

1.2 Discovery of Neutrons 9

1.3 Fermi Model of β Decay 11

1.4 Experiments to Discover Neutrino Properties 12

1.4.1 Rodeback & Allen Experiment 12

1.4.2 Reines & Cowan Experiment (Discovery of Neutrino) . . . 13

1.4.3 Ray Davis Experiment (Are Neutrinos and Anti-neutrinos Same Particles?) 14

1.4.4 Discovery of Muon Neutrinos (ν_μ) 16

1.4.4.1 Muon Decaying to Neutrinos ($\mu \to e + 2\nu$) . . 18

1.4.5 Discovery of Tau Neutrino (ν_τ) 19

1.4.6 How Many Flavors of Neutrino Are There? 20

1.5 Discovering and Understanding Neutrino Anomalies 20

1.5.1 Solar Neutrino Anomaly 20

1.5.2 Atmospheric Neutrino Anomaly 27
1.5.3 Neutrino Oscillations 28
1.5.3.1 Neutrino Oscillations in Vacuum 29
1.5.3.2 Neutrino Oscillations With Two Flavors . . . 33
2 TEXONO EXPERIMENT 37
2.1 Kuo-Sheng Neutrino Laboratory 37
2.2 ULB-HP Ge DETECTOR 39
2.3 CsI (Tl) Crystal Scintillating Detector 43
3 BEYOND THE STANDARD MODEL PHYSICS SEARCH WITH NEUTRINO ELECTRON SCATTERING 47
3.1 Neutrino Electron Scattering in Standard Model 47
3.2 Non Standard Interactions of Neutrinos 49
3.3 Unparticle Physics 52
3.3.1 Neutrino-Electron Scattering via Unparticle Exchange . . 53
4 ANALYSIS AND RESULTS 55
4.0.2 Non-Standard Neutrino Interactions 58
4.0.3 Unparticle Physics Parameters 60
REFERENCES 66

LIST OF TABLES

TABLES

Table 1.1 Some selected experimental limits on lepton-number-violating processes. (Adopted from [34, 40].) 19

Table 1.2 Nuclear reactions responsible for producing almost all of the Sun's energy and the different "types" of solar neutrinos (nomenclature): pp-neutrinos, pep-neutrinos, hep-neutrinos, ^{7}Be-neutrinos, and ^{8}B-neutrinos. 'Termination' refers to the fraction of interacting protons that participate in the process. (Adopted from [17, 45].) 22

Table 1.3 Summary of R measurements.([17, 54]) 28

Table 2.1 Summary of the key information on the three data taking periods with 1.06 kg HPGe detector which is used for neutrino magnetic moment search. (Adopted from [62]). 39

Table 2.2 Summary of the key information of the four data taking periods with CsI (Tl) scintillation crystal to measure cross-section of $\bar{\nu}_e - e^-$ scattering. The period numbering follows the same scheme as in Ref [62]. (Adopted from [61].) 39

Table 4.1 Constraints at 90% CL due to one-parameter fits on the NSI couplings. The results are presented as "best-fit ± statistical error ± systematic error". Bounds from LSND [99] and combined data [100], as well as from a model-independent analysis [108] are compared with those of this work. The projected statistical sensitivities correspond to a potential measurement of the SM cross-section at 2% accuracy [61]. 61

LIST OF FIGURES

FIGURES

Figure 1.1 Continuous β spectrum of RaE. (Adopted from [13]) 4

Figure 1.2 α rays emitted from Po source collide with the Be and a new highly penetrating radiation (purple arrows) comes out. This radiation interacts with the protons in the paraffin layer and cause to protons to leave the paraffin. These free protons are observed with the cloud chamber. (This picture is adopted from [25]) 10

Figure 1.3 Fermi explains β decay as a neutron decaying into a proton, electron and antineutrino. 11

Figure 1.4 Schematic view of the experimental set up for the detection of anti neutrinos. (Adopted from [31]) 13

Figure 1.5 Schematic view of AGS neutrino experiment. (Adopted from [34].) 17

Figure 1.6 Cross section of the reaction $e^- + e^+ \rightarrow hadrons$ as a function of cm energy. The results belong to experiments ALEPH, DELPHI, L3 and OPAL. The red curves describes the Standard Model predictions for two and four light neutrino flavours. (Adopted from [44]) 21

Figure 1.7 Schematic representation of CNO cyle. This also burns hydrogen to helium with C, N and O acting as catalysts and is responsible for 1.6% of the solar energy.(Adopted from [34]) 21

Figure 1.8 Contributions of the CNO cyle and pp chain for energy production in stars as a function of the central temperature. (Adopted from [34]) 23

Figure 1.9 The predicted solar neutrino energy spectrum. The figure shows the energy spectrum of solar neutrinos predicted by the most recent version of the standard solar model. For continuum sources, the neutrino fluxes are given in number of neutrinos $cm^{-2}s^{-1}$ MeV^{-1} at the Earth's surface. For line sources, the units are number of neutrinos $cm^{-2}s^{-1}$. Total theoretical uncertainties are shown for each source. (Adopted from [17].) 24

Figure 1.10 Predictions of the standard solar model and the total observed rates in the six solar neutrino experiments: chlorine, SuperKamiokande, Kamiokande, GALLEX, SAGE, and SNO. The model predictions are color coded with different colors for the different predicted neutrino components. For both the experimental values and the predictions, the 1 sigma uncertainties are indicated by cross hatching.(Adopted from [17].) 26

Figure 1.11 Neutrino flavor change (oscillation) in vacuum. "Amp" denotes an amplitude.(Taken from [57]) 30

Figure 1.12 Present situation of oscillation parameters. 35

Figure 2.1 Schematic layout of the Kuo-Sheng Neutrino Laboratory together with the reactor core and building. (Adopted from [61].) 38

Figure 2.2 The shielding design of KSNL. Similar structures apply to the back and front walls. Detectors and inner shieldings were placed in the inner target volume (Adopted from [61].) 40

Figure 2.3 Schematic layout of the HPGe with its anti-Compton detectors as well as inner shieldings and radon purge system. (Adopted from [62].) 40

Figure 2.4 Schematic layout of the electronics and data acquisition systems of the HP-Ge and the associated ACV and CRV detectors.(Adopted from [62].) 41

Figure 2.5 Selection procedures of the recorded data : (a) pulse shape analysis, (b) anti-Compton selection, and (c) cosmic-ray veto. (Adopted from [62].) 42

Figure 2.6 The residual plot on the Reactor ON data of all periods combined over the background spectra. (Adopted from [62].) 43

Figure 2.7 Schematic drawing of the CsI (Tl) scintillating crystal array. Light output is recorded by PMTs at both end. (Adopted from [61].) 44

Figure 2.8 Typical Q_L versus Q_R distribution for H1(CRV) events showing the background events of natural sources. Different colors denote whether the PMT signals are saturated at their FADC readout or not. Additional software routines were devised to provide correct energy information for saturated events. (Adopted from [61].) 45

Figure 2.9 The combined residual spectrum $[R_{expt}(\nu) = R_{\mathrm{H1}}(\mathrm{ON}) - R_{\mathrm{H1}}(\mathrm{BKG})]$ in the 3−8 MeV energy region. The blue and red lines correspond to the SM expectations and to the best-fit of the data, respectively. (Adopted from [61].) 46

Figure 3.1 $\nu_\mu - e^-$ scattering can only take place via Neutral Current. 47

Figure 3.2 Apart from the $\nu_\mu - e^-$ scattering $\bar{\nu}_e - e^-$ scattering can take place both Charged current (CC) and Neutral Current (NC). 48

Figure 3.3 Both lepton number violation and neutrino oscillation phenomena could be an explanation of atmospheric and solar neutrino anomaly. The possibilities that occur in source (above) and detector (below) is shown. 50

Figure 3.4 NSI of neutrinos can be written as a model independent way like four fermi interaction with new couplings. 51

Figure 3.5 Interactions of neutrino with electron via exchange of virtual scalar $\mathcal{U}_\mathcal{S}$ and vector $\mathcal{U}_\mathcal{V}$ unparticle. 53

Figure 4.1 The three data sets adopted for this analysis. Observable NSI or UP spectra at allowed and excluded parameter space are superimposed. Top: (a) DS1-CsI(Tl) Reactor ON−OFF [62], showing SM+NSI with NSI at $(\varepsilon_{\mathrm{ee}}^{\mathrm{eR}}, \varepsilon_{\mathrm{ee}}^{\mathrm{eL}}) = (0.1,0.1)$ and $(0.05,-0.05)$. Middle: (b) DS2-HPGe Reactor ON−OFF [61], showing SM+UP with $\lambda_0 = 4\times10^{-6}$ versus 3×10^{-6} at $d_\mathcal{S} = 1.01$. Bottom: (c) DS3-ULEGe Reactor ON only [6], showing SM+UP with $\lambda_0 = 1.2\times10^{-5}$ versus 6.5×10^{-6} at $d_\mathcal{S} = 1.01$. The SM contributions from $\bar{\nu}_\mathrm{e}$−e are displayed in (a) and (b) as comparison, and are out of range at $\sim 10^{-3}$ kg^{-1}keV^{-1}day^{-1} in (c). 57

Figure 4.2 Differential cross-section as function of the recoil energy T with typical reactor-$\bar{\nu}_\mathrm{e}$ spectra. NSI at coupling parameters relevant to this work using CsI(Tl) as target is shown. 58

Figure 4.3 The allowed region at 90% CL for NU NSI parameters of ε_{ee}^{eL} and ε_{ee}^{eR}; The allowed regions from the LSND experiment on ν_e−e are superimposed. 59

Figure 4.4 FC NSI parameters of $\varepsilon_{e\tau}^{eL}$ and $\varepsilon_{e\tau}^{eR}$ from DS1-CsI(Tl) on $\bar{\nu}_e$−e. The allowed regions from the LSND experiment on ν_e−e are superimposed. 60

Figure 4.5 Differential cross-section as function of the recoil energy T with typical reactor-$\bar{\nu}_e$ spectra. Scalar UP, at two values of $(d_{\mathcal{S}}, \lambda_0)$ and vector UP, at a value of $(d_{\mathcal{V}}, \lambda_1)$ for both FV and FC cases, using Ge as target. The SM contributions are also superimposed. The relevant energy ranges of the three data sets used in the present analysis are also shown. 62

Figure 4.6 Constraints on UP with scalar exchange. The coupling λ_0 versus mass dimension $d_{\mathcal{S}}$ at $\Lambda_{\mathcal{U}} = 1$ TeV are shown; Parameter space above the lines is excluded. 63

Figure 4.7 Constraints on UP with scalar exchange. Upper bounds on λ_0 at different energy scales $\Lambda_{\mathcal{U}}$ are displayed. Parameter space above the lines is excluded. . . 63

Figure 4.8 Constraints on UP with vector unparticle exchange − The coupling λ_1 versus $d_{\mathcal{V}}$ at $\Lambda_{\mathcal{U}} = 1$ TeV. The bounds apply for both FV and FC cases. 64

Figure 4.9 Constraints on UP with vector UP exchange. Upper bounds on λ_1 at different energy scales $\Lambda_{\mathcal{U}}$ for FV and FC couplings, respectively, at two values of $d_{\mathcal{V}}$. Parameter space above the lines is excluded. 65

CHAPTER 1

INTRODUCTION

There are four known fundamental interactions in nature; electromagnetic, weak, strong and gravitational. Electromagnetic interactions are responsible for the forces between charged particles, weak interaction is the reason of radioactive β decay of unstable nuclei and explains how neutrinos interact with matter, strong interaction binds quarks together and explains how protons and neutrons can stay together in nucleus and gravity which is the most famous and weakest one among them is the reason of the falling of apple to Newton's head. All these interactions except from gravity are described by quantum fields which manifest themselves as particles. Also there are continuing hard studies to describe the gravity with quantum fields in order to unify all these forces like; String theory, loop quantum gravity, supergravity, etc. However, they have not been verified yet.

Standard Model (SM), which is based on these quantum fields, is very successful in explaining the most of the experimental data obtained up to now, which means SM is tested between the energy ranges in which experiments are performed. The SM is planned to be tested on LHC [1] up to energy levels of 14 TeV as well as low energy threshold experiments in neutrino nucleus coherent scattering [2, 3, 4].

Although SM seems so successful, there are still some key concepts where SM fails to explain. One of them is the Dark Matter problem and lots of experiments are being performed to solve this mystery [5, 6]. Neutrinos being massive is the another important phenomena which can not be explained by SM. The strong evidence of neutrino oscillation depending on the solar and atmospheric neutrino experiments as well as long-baseline accelerator and reactor data have been confirmed. Neutrino oscillation phenomena implies neutrinos being massive and therefore neutrino mixing [7]. The massive neutrino models lead to modifications of SM elec-

troweak interaction so that neutrinos might have new interactions. Existing of non-standard interaction is important in the sense that, it will affect the neutrino oscillation parameters and astrophysics, like it may change the understanding of supernova explosion [8].

These are some of the reasons why we need theories beyond the SM. It seems to me that, there are two kinds of Beyond the Standard Model theories. One kind is the candidates trying to solve unexplained phenomena such as Dark Matter and neutrinos being massive and the other kind is the theories that depend on "Why not?". Searching for Non-Standard Interactions of neutrinos and models in which neutrinos gain mass can be put in the first category. However, Unparticles which emerged while Georgi was "playing" with scale invariant theories, depend on the reliability of mathematical equations and can be put in the second category. There is no reason that Unparticle must exist however there is not also any reason why it should not. All these beyond the standard models which can be tested by experiments should be searched since these new theories will increase the knowledge of how nature behaves.

$\nu_e(\bar{\nu}_e)$ scattering of electrons have played very important roles in testing SM and the searches of neutrino intrinsic properties as well as understanding the neutrino oscillation. Neutrino electron scattering experiments, which are originally designed for measurement of the cross-section or identifying the intrinsic properties of neutrino provides a good tool to test SM and search for the Beyond the SM theories such as NSI of neutrinos and Unparticle physics.

There are so many beyond the SM theories like, Supersymmetry, grand unified theories, leptoquarks, extra dimension an so on, which all depend on the quantum fields that may give rise to new particles which are expecting to be observed in LHC. However, other types of quantum fields may exist as well. Banks Zaks studied about the scale invariant fields which claims that there are non-integer number of fermion generation in nature [9]. Depending on the Banks-Zaks theory, in 2007, H.Georgi proposed that Banks-Zaks Fields and SM fields can both exist in some high energy scale and these two sectors can interact with each other by a messenger particle with a high mass scale [10, 11]. By means of the interaction with SM fields, it is possible to search for quantitative results related with unparticle. Both of the theories contribute to the cross section of $\nu_e(\bar{\nu}_e)$ scattering that SM predicts. And looking for the excess number of events than SM predicts, it is possible to put bounds for NSI and Unparticle parameters.

In this study, two of the Beyond the Standard Model physics; Non-Standard Interaction of

neutrinos and Unparticle physics effects, are searched with $\bar{\nu}_e - e^-$ scattering experiments which are conducted by TEXONO Collaboration. The thesis is organized as follows; In Chapter 1, a brief history of neutrino physics starting with the discovery of continuous β decay is explained. How the idea of neutrinos arose and how such an elusive particle which was thought as undiscoverable even by the owner of the idea of existence of neutrino is discovered is tried to be explained. Moreover, information about how the properties of such very weakly interacting neutrinos are discovered both theoretically and experimentally is given. Furthermore, in this chapter the atmospheric and solar neutrino anomalies which can not be answered by Standard Model is mentioned and information about neutrino oscillations is given. In chapter 2, TEXONO experiment is explained briefly. In the third chapter, first, the physics of $\nu_e(\bar{\nu}_e)$ scattering with respect to electroweak interaction is given and later it is explained that how $\nu_e(\bar{\nu}_e)$ cross section modifies if the Non-Standard Interaction and Unparticle physics exist. And Finally, in Chapter 4, analysis of Texono data is explained and the results for Non-standard interaction and unparticle parameters are shown and these results are compared with the other experiments.

1.1 β Decay Anomaly

In 1914, James Chadwick [12] measured the kinetic energy of electrons emitted in the β decay of RaB (which is now known as ^{214}Pb) using magnetic spectrometer. The emitted electrons are put in a magnetic field and hence the electrons are deflected depending on their velocities according to the relation;

$$q\vec{v} \times \vec{B} = \frac{mv^2}{R} \tag{1.1}$$

$$R = \frac{qB}{mv} \tag{1.2}$$

What he observed was, different from the α and γ rays, which are consisted of mono-energetic lines, β rays had continuous spectra (Fig. 1.1). In every measurement the equation in (1.2) give different results.

At that time, depending on the result of some experiments, it was also believed that, the electrons emitted in β decay had mono-energetic line too. However, the reason of mono-energetic line spectrum is explained by internal conversion. An excited nucleus emits γ rays

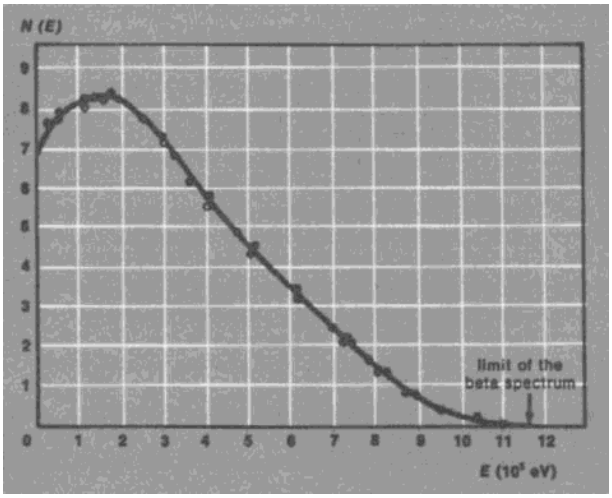

Figure 1.1: Continuous β spectrum of RaE. (Adopted from [13])

and these rays interact with the electrons in the outer shell of the atom and cause the electrons to be ejected with high speed from the atom. In fact, these electrons can not be considered as β particles, since the atomic number of nucleus does not change in this process and therefore it is not a nuclear process. Moreover, some nuclei like RaE (^{210}Bi) do not emit γ rays and in this case mono-energetic lines of electrons can not be observed since internal conversion process can not take place and the spectrum is continuous.

To check the results, Chadwick repeated the experiment and this time, instead of using magnetic spectra, he measured the kinetic energy of electrons by measuring the ionization energy. However, the result was again continuous spectra. In a two body decay, $A \longrightarrow B+C$ (which is thought the case for the β decay), the energy of the emitted particle is found using relativistic four-momentum calculation as below;

$$p_A = p_B + p_C, \tag{1.3}$$

$$p_C = p_A - p_B, \tag{1.4}$$

$$p_C{}^2 = p_A{}^2 + p_B{}^2 - 2p_A p_B, \tag{1.5}$$

$$m_C{}^2c^2 = m_A{}^2c^2 + m_B{}^2c^2 - 2m_A E_B, \tag{1.6}$$

$$\Rightarrow E_B = \frac{(m_A{}^2 + m_B{}^2 - m_C{}^2)c^2}{2m_A} \tag{1.7}$$

where m corresponds to mass of the particles and p corresponds to four momentum of the particles. Since the masses are constant, it is expected that β particles should have mono-

energetic line spectrum. One of the ideas to explain this weirdness was that, the reason could be due to secondary process. Electrons emitted from a nucleus could have lost its energy in different amounts due to the interactions with other nuclei while passing through the material. It is nearly impossible to acquire pure radioactive source. Radioactive source generally consists of some stable nuclei which exists due to the decay of some other radioactive nuclei and also it may consist some other radioactive nuclei that is not decayed yet. Due to this variety, electrons emitted from nuclei could have interacted with these various nuclei and lose its energy with different amounts. In this case, why do α particles have mono-energetic lines ? α particles also pass through the material in which different nuclei exist, but, since α particles are so heavy that they did not interact so easily like electrons α particle spectrum expected to be mono-energetic. Besides, L.Meitner, who was a big supporter of this idea, Rutherford, von Bayer and Otto Hahn also shared the same idea.

On the contrary, D.Ellis [14] claimed that the continuous spectrum is due to the primary electrons emitted from the nucleus. To test these ideas, Ellis tried to measure the total energy of emitted electrons from β decay of RaE. Chadwick had measured only the kinetic energy of electrons and missed the information about the energy dissipated as heat. If the electrons are primary electrons, the expected energy value should be closer to the mean energy that Chadwick measured. On the other side, if the electrons are secondary then the expected energy will be the value of the highest kinetic energy as Chadwick observed. J.D Ellis and W.A. Wooster [15] in 1927 did the experiment by putting the radioactive sample in a heat calorimeter. The result for each decay was, in terms of Volts, a heat of 344000 ± %10 V which corresponded to mean energy that Chadwick measured. Therefore, this result became a strong evidence for considering the electrons emitted from β decay as primary ones. However, Ellis explained that there might be continuous γ spectrum which can not be detected by heat calorimeter, therefore it could not be said certainly that electrons are primary.

Meitner was not convinced with the experimental result and designed a new set-up with improved apparatus. What she measured was 337000 ± %6 V confirming the result of Ellis. Furthermore, using a different set-up, using ionization tubes, Meitner [16] proved that γ spectrum does not exist and confirmed that the β^- particles are primary. As a consequence, it was proved that the electrons emitted due to β decay had continuous spectrum and the reason was waiting to be found.

1.1.1 Spin Statistics problem of β Decay

What was the sources of the electrons emitted in β decay? There were some theories about the structure of the nucleus at that time, for instance α particles were considered to be the fundamental particles of nuclear constituents [17]. However, the most accepted model after the Rutherford's famous scattering experiment [18] was this; nucleus consisted of protons and electrons in a way that make the nucleus positive. For instance, ^{14}N nucleus consisted of 14 protons and 7 electrons which makes nuclear charge +7e. Moreover, ^{7}Li nucleus consisted of 7 protons and 4 electrons making nuclear charge with +3e. There were some problems with this theory. One of them was about spin statistics theorem which emerged with the development of quantum and wave mechanics. Spin integer particles are described with symmetric wave functions and called as bosons. On the other hand, spin half particles are described with anti symmetric wave functions and called as fermions. Moreover, if the composite particle consists of even number of fermions then it is called as boson, if it consists of odd number of fermions then it is called as fermion. Therefore, according to this nuclei model, nitrogen nuclei which consisted of $14p + 7e = 21$ fermions, expected to behave as fermion. However, using the band spectra R.Kronig [19] and W.Heitler and G.Herzberg [20] showed experimentally that Nitrogen has bose statistics. The similar unexpected result was of the Li nucleus, which expected to have $7p+4e = 11$ fermions to act as a fermion. However, it was shown that Li nuclei had spin 1 and bose statistics. Therefore, these phenomena could not be explained by this nuclear model.

Another problem related to this nuclei model was about the magnetic moment of the nuclei. It was known at that time, the magnetic moment of proton was much smaller than the electron. Moreover, magnetic moment of electron is much larger than the magnetic moment of nucleus. Then the question arises. How can the magnetic moment of electrons can be bigger than the nuclei which consists of both electrons and protons? This was also waiting to be answered.

There was one more problem with this model; the observed kinetic energy of electrons emitted in β decay. If the nucleus consisted of electrons, by a rough calculation it is easy to find the energy of electrons inside the nucleus. Using uncertainty relation and taking the nucleus size

as $1fm$, we find the momentum of the electron as;

$$\Delta x \, \Delta p \geq \frac{\hbar}{2}, \tag{1.8}$$

$$x \approx 1fm, \tag{1.9}$$

$$E \approx pc \approx 100 \; MeV. \tag{1.10}$$

The observed kinetic energy is much less than this as shown in Figure 1.1. Hence, it seems nucleus can not contain electrons or electrons emitted in β decay do not come from nucleus.

1.1.1.1 The Idea of Neutrino

One of the ideas to answer these anomalies, belonged to Bohr, who liked "arguing" with Einstein [21]. The electrons inside the nucleus have different characteristics than the free electrons. These bound electrons do not behave as ordinary fermions and interact in a way that violate conservation of energy and momentum. In other words, energy conservation is statistically valid over the many event but not at the level of individual atomic decay [22].

Apart from the quantum mechanical debates with Einstein, Bohr was wrong this time. The idea that rescued the conservation of energy and momentum, came from Wolfgang Pauli, with his famous letter to a physics conference which is held in Tubingen, Germany, in 1930. The letter as it takes place in [22] is like this;
"Dear Radioactive Ladies and Gentlemen,
As the bearer of these lines, to whom I graciously ask you to listen, will explain to you in more detail, how because of the "wrong" statistics of the N and ^6Li nuclei and the continuous β-spectrum, I have hit upon a desperate remedy to save the "exchange theorem" of statistics and the law of conservation of energy. Namely, the possibility that there could exist in the nuclei electrically neutral particles, that I wish to call neutrons, which have spin $1/2$ and obey the exclusion principle and which further differ from light quanta in that they do not travel with the velocity of light. The mass of the neutrons should be of the same order of magnitude as the electron mass and in any event not larger than 0.01 proton masses. The continuous β-spectrum would then become understandable by the assumption that in β decay, a neutron is emitted in addition to the electron such that the sum of the energies of the neutron and electron is constant. Now the question that has to be dealt with is which forces act on the neutrons? The most likely model for the neutron seems to me, because of wave mechanical reasons (the

details are known by the bearer of these lines), that the neutron at rest is a magnetic dipole of a certain moment μ. The experiments seem to require that the effect of the ionization of such a neutron can not be larger than that of a γ ray and then μ should not be larger than $e * 10^{-13}$ cm.

For the moment, however, I do not dare to publish anything on this idea and I put to you, dear Radioactives, the question of what the situation would be if one such neutron were detected experimentally, if it would have a penetrating power similar to, or about 10 times larger than, a γ ray.

I admit that on a first look my way out might seem to be unlikely, since one would certainly have seen the neutrons by now if they existed. But nothing ventured nothing gained, and the seriousness of the matter with the continuous β spectrum is illustrated by a quotation of my honored predecessor in office, Mr. Debey, who recently told me in Brussels : "Oh, it is best not to think about it, like the new taxes." Therefore one should earnestly discuss each way of salvation. So, dear Radioactives, examine and judge it. Unfortunately I can not appear in Tübingen personally, since I am indispensable here in Zürich because of a ball on the night of 6/7 December. With my best regards to you, and also to Mr. Back, your humble servant,
W. Pauli "

Pauli, with proposing a new neutral particle, which he named as neutron, has the property of being fermion, interacting very weakly with matter and weighing less than %1 of the proton, supplied a good candidate theory to solve the anomalies of β decay. With this proposal the nitrogen nuclei would consist of $^{14}N = 14p + 7e + 7\ ''neutron''$ with a total 28 fermion which acts as a boson as expected. Hence, with this new hypothetical particle spin statistic problem seems to be solved.

With this new neutral particle, β decay of nucleus thought to occur like this; $^{A}Z \rightarrow^{A} (Z + 1) + e^{-} + \ ''neutron''$ where A and Z correspond to atomic mass number and charge of the nucleus respectively. Mother nucleus decayed into a daughter nucleus by emitting an electron and neutron, therefore charge of the daughter nucleus increased by one unit as consistent with charge conservation. With this three body decay, Pauli had explained not only the continuous energy spectrum of β^{-} particles but also guaranteed the maximal energy of electrons being always less than the mass difference between mother and daughter nuclei. If this neutral particle takes the energy in different amounts away then continuous spectrum of β decay

would have been understood. After thinking about the empirical masses of the mother and daughter nuclei, Pauli discarded the idea that "neutron" was one of the constituents of nuclei. Pauli did not publish his idea since the new particle interacted so weakly with matter and seemed impossible to detect.

1.2 Discovery of Neutrons

In 1912, J.J Thompson discovered what we now know as isotopes by pointing out that natural neon gas is a mixture of two kinds of elements. Moreover, he pointed out that these elements have different atomic weights. In the following years, it had been understood that many of the elements are mixtures of two or more kinds of isotopes. Isotopes have the same atomic number (number of protons) which mean same nuclear charge, same chemical properties but having different atomic masses. Since the nuclei is consisted of same number of protons, which is $\approx$ 2000 times heavier than electron, what could be the reason for the change in atomic masses?

Rutherford explained his ideas about the possibility of a neutral particle which has similar mass of a proton inside the nucleus, in his Bakerian Lecture, in 1920 [23]. This could be a solution to understand the isotopes. Rutherford was the first one who believed neutron existed, with basic instinct. (The existence of new neutral particle would have solved the spin statistics problem either.) Apart from the discoveries which are made in one day such as radioactivity, X-rays the discovery of neutron took two years.

In 1928, Walter Bothe and his student H.Becker were studying the radiation emitted from a Be source which is bombarded with α particles coming from the Polonium source. They discovered a neutral and high penetrating radiation which they thought that it should have been gamma rays. Later, they also showed that the similar radiation is also emitted when Lithium and Boron is used as a target. Moreover, they measured the energy of this highly penetrating rays by calculating the absorption coefficient and found out that these rays were very energetic, even more than the energy of α particles. This result implied that either energy is not conserved or nuclear disintegration took place and this was an unexplained phenomena at that time.

Irene Curie and Frederic Joliot who are daughter and groom of Marie Curie, discovered in

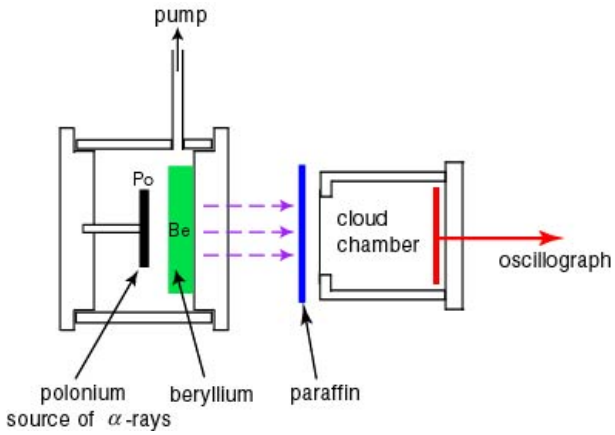

Figure 1.2: α rays emitted from Po source collide with the Be and a new highly penetrating radiation (purple arrows) comes out. This radiation interacts with the protons in the paraffin layer and cause to protons to leave the paraffin. These free protons are observed with the cloud chamber. (This picture is adopted from [25])

1932 that these highly penetrating rays were able to eject protons from a paraffin layer (Figure 1.2). However, maybe due to the bias they have in their minds, they thought that these rays were gamma rays. They interpreted this phenomena as Compton effect; gamma rays are scattered from the protons and protons are recoiled and left the paraffin layer. Since protons are 1836 times heavier than electrons, it is not so easy to recoil protons with gamma rays. For this to happen, gamma rays had to be very energetic. Since they measured the kinetic energy of protons as 5.3 MeV, the photon energy should be around 50 MeV to be able to eject protons. When the results are published, Rutherford told that he did not believe the proposed solution [24]. When Ettore Majorana read the paper, he said with his sarcastic spirit "What fools. They have discovered the neutral proton and they do not recognize it". [24]

Chadwick, who was a student and colleague of Rutherford, repeated the experiment. He used Polonium and Beryllium as a source and with this he acquired the neutral radiation (Figure 1.2). In addition to paraffin, he used helium and nitrogen as a target too. Comparing the results of different targets and assuming the new particle has the same velocity as proton he managed to measure the mass of the new particle as 938 ± 1.8 MeV/c^2 [26] which is so close to the present results $m_n = 939.57$ MeV/c^2. Since the particle was neutral and due to the similarity in name prot**on** and electr**on**, Chadwick named this new particle as neutron in 1932. He was rewarded with a Nobel prize with discovery of neutrons in 1935. However, it is important to note that this particle is not the same particle as Pauli proposed to explain β spectrum anomaly.

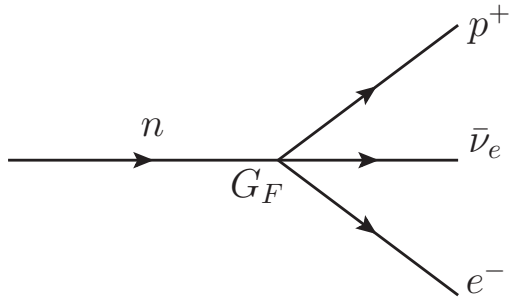

Figure 1.3: Fermi explains β decay as a neutron decaying into a proton, electron and antineutrino.

1.3 Fermi Model of β Decay

Up to 1930, it was believed that nucleus is consisted of protons and electrons with a total positive charge. This model tried to explain the origin of electrons emitted in β decay also. However, there were spin statistics problem and the measured energy of emitted electrons in β decay was much less than the expected. With the discovery of neutron, D. Ivanenko and W. Heisenberg proposed a model independently that nuclei is consisted of neutrons and protons only. In this model, nucleus of nitrogen is consisted of $7p + 7n$ which satisfies the need of the nucleus charge and mass. Moreover, this model solves the spin statistics problem. Furthermore, the idea that nucleus did not contain electron also solved the magnetic moment anomaly mentioned earlier. Although this model answered the anomalies of nucleus, a new problem emerged. Which force enables to hold the nucleons together inside the nucleus? Since protons repel each other, there should have been a new force (which we now know as strong interaction) balancing the electromagnetic interaction.

Before the discovery of neutron, Pauli had proposed that there may be a neutral, spin 1/2, so light and weakly interacting particle emitted in β decay. In 1934, Enrico Fermi [27, 28], by considering the Pauli's proposed particle, developed a four Fermi interaction of β decay using the Quantum Electrodynamic. With this new theory, neutrons could decay into proton, electron and neutrino (Figure 1.3). Thus, the source of electrons in β decay would have been understood. Although electrons do not exist in nucleus, they emerge from the neutron decay. Moreover, existence of neutrons explain the continuous spectrum of β decay. Neutrinos could take away a different amount of the energy with each decay, sometimes leaving less and sometimes leaving more for the electron. The interaction of neutron decay, $n \rightarrow p + e + \nu_e$

was described as; [17]

$$\frac{G_F}{\sqrt{2}}(\bar{n}\Gamma_N p)(\bar{\nu_e}\Gamma_L e) + H.c \tag{1.11}$$

where G_F is the dimensionful Fermi constant which defines the strength of the interaction and $\Gamma_{N,L}$ are the linear combination of γ matrices $(1, \gamma^5, \gamma^\mu, \sigma_{\mu\nu})$. After Chadwick's discovery of neutron, Fermi changed the name of Pauli's particle as neutrino, in which "ino" suffix is used to represent the diminutive in Italian. Finally, with Fermi's model, the mystery of the continuous spectrum of β decay would have been explained if the neutrino existed.

1.4 Experiments to Discover Neutrino Properties

1.4.1 Rodeback & Allen Experiment

The first signatures of existence of neutrinos was the nuclear recoil experiment carried by G.W Rodeback and J.S Allen [29] in 1952. This experiment also proved that only one neutrino is emitted instead of three or more in β decay. The interaction to be searched was electron capture of ^{37}Ar atom; a proton is turned into a neutron by capturing the electron and a neutrino is emitted.

$$^{37}Ar + e^- \rightarrow^{37} Cl + \nu_e + Q$$

where Q is the disintegration energy, e^- is the auger electron, captured orbital electron. Since the recoil of the orbital electrons can be neglected, due to momentum conservation, the recoil momentum of ^{37}Cl is directly related to emitted neutrinos. Assuming the neutrino is massless the disintegration energy depends on the mass difference of $^{37}Ar \leftrightarrow^{37} Cl$ which gives $Q \approx 816$ keV. If there is only one neutrino emitted in this reaction, then the disintegration energy is shared only between the recoil energy of the ^{37}Cl and the neutrino. Since there are two particles in the final state and $M_{Cl} \geq Q \approx E_\nu$ then recoil energy of Cl is given by;

$$T_{Cl} = \frac{{E_\nu}^2}{2M_Cl} \approx \frac{Q^2}{2M_{Cl}} = 9.67 \pm 0.08eV \tag{1.12}$$

Recoiling Kinetic Energy of Cl corresponds to a velocity of 0.71 ± 0.04 cm/μsec. Therefore, a delayed coincidence measurement enables to measure the recoil velocity. Recoil energy is measured as $T_{Cl} = 9.63 \pm 0.03$ eV which fits well with the result in equation 1.12. Although this experiment is not a direct detection of neutrinos, the results point out that experimental results fits well with the existence of neutrino and moreover show that number of neutrinos

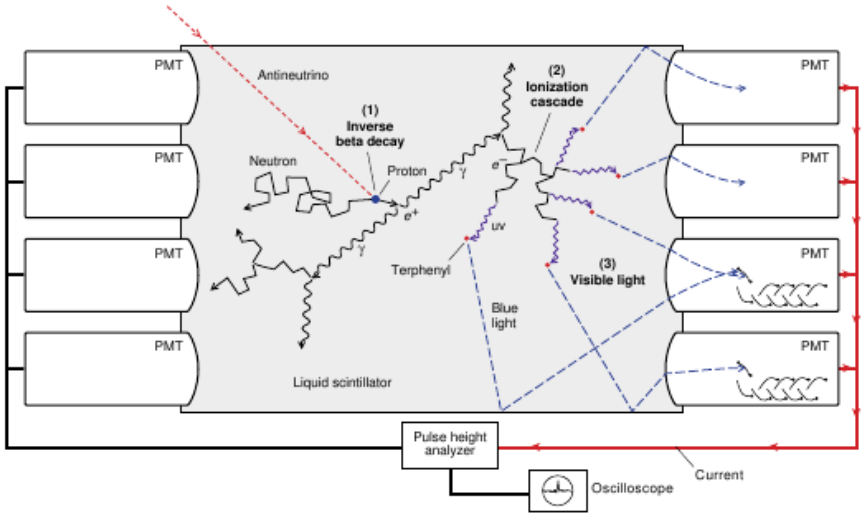

Figure 1.4: Schematic view of the experimental set up for the detection of anti neutrinos. (Adopted from [31])

emitted in this reaction is one, which is an answer of question how we could be sure about how many neutrinos are emitted in a reaction.

1.4.2 Reines & Cowan Experiment (Discovery of Neutrino)

Although Pauli proposed that existence of neutrino solves the mystery of β decay, he still had suspects about it. Once he said; " I have done something very bad today by proposing a particle that can not be detected; it is something no theorist should ever do" [30]. However, F.Reines and C.L Cowan accepted the challenge and designed an experiment to discover neutrino. First of all, since neutrinos are weakly interacting particles and the cross sections is so small, they needed an intense source of neutrinos. With the invention of nuclear reactors, it became possible to acquire high neutrino flux which is around 10^{20} neutrinos per second. Theoretically, if β decay is due to conversion of neutron to proton, electron and antineutrino ($n \rightarrow p + e^- + \bar{\nu}_e$), then the reaction $p + \bar{\nu}_e \rightarrow n + e^+$ should also take place too. Moreover, since the neutrino source is available due to fission reaction of Uranium, it is the only possibility to acquire anti-neutrinos. Owing to this, using the anti neutrinos was the only way to search neutrino properties at that time . In 1953, Reines and Cowan designed an experiment near the Hanford reactor to search the interaction of $p + \bar{\nu}_e \rightarrow n + e^+$. As shown in Figure 1.4; they used $CdCl_2$ dissolved in a water tank and the tank is surrounded by two liquid scintillators which is a chemical compound that emits short light pulses when a charged particle

passes through. The tank is surrounded with photomultiplier tubes which are sensitive to the scintillators small light pulses. When anti-neutrino interacted with protons then neutrons and positrons are emitted. After a finite time interval, neutrons are absorbed by ^{113}Cd and becomes ^{114}Cd. This new radioactive nucleus emits a photon which is recorded by detectors. Moreover, emerged positrons interact with the electrons and due to pair annihilation 0.511 MeV photons are emitted. These photons are also recorded by scintillators. There is an exact time difference between these signals (one emitted due to pair annihilation and one due to neutron absorption). Therefore, they started to wait for double signal separated in an exact time difference. The reliable results are acquired in 1956. They observed neutrinos 0.56 ± 0.06 count/hour [32]. To be able to perform double checks, they looked at the number of observed events when the reactor is at its highest power setting. In this case, they expected to observe more events. The results were 2.88 ± 0.12 count/hour which was 20 times of the accidental noise level. For one more test, instead of water they used heavy water (D_2O). The role of heavy water is that it slows down the neutrons and this makes them easy to detect. Thus, it is expected to observe more neutrinos and this was the case. With these checks, neutrino had been directly observed. After the discovery, Reines and Cowan sent a telegram to Pauli in Zurich, in 1956, about the discovery of the Pauli's "ghost particle". "We are happy to inform you that we have definitely detected neutrinos" [30]. They won the Nobel prize with this discover in 1995 for "pioneering experimental contributions to lepton physics".

1.4.3 Ray Davis Experiment (Are Neutrinos and Anti-neutrinos Same Particles?)

The property that differs between particle and antiparticle is the charge that they have. But what happens if the particle is neutral like neutrinos? Is it the case that neutrinos and anti-neutrinos are same particles, like photon and π^0 which are their own antiparticles? Emitted neutrinos in β decays are neutrinos or anti-neutrinos? These questions were important to be able to understand neutrino interactions with matter.

Pontecorvo, who was a student of Fermi, proposed an alternative way to Reines and Cowan experiment in 1945 to detect neutrinos. When neutrino interacted with nucleus, the nucleus will transpose into another since neutrons will transpose into protons after the interaction.

$$n + \nu \rightarrow p + e^- \tag{1.13}$$

Hence, it would be easy to observe the new element which existed after the neutrino interac-

tion. Pontecorvo's idea to observe neutrino was looking for the interaction;

$$^{37}Cl + \nu \rightarrow ^{37}Ar + e^{-}$$

In 1955, R.Davis [33], who was a radiochemist at Brookhaven National Laboratory, designed an experiment to observe neutrinos by Pontecorvo's method by using the nuclear reactor as neutrino sources.

When neutrino is captured by ^{37}Cl, ^{37}Ar is expected to form. And since this is a radioactive isotope, it decays back to ^{37}Cl by inverse reaction with a half time of 35 days. As a target material 3800 liters of CCl_4, tetrachloride was used in this experiment. To be able to extract the produced Ar atoms, he passed He gases through the liquid and then freeze out the Ar atoms in a cooled charcoal trap [34].

Surprisingly, he was not able to measure the cross section therefore he put an upper bound for it as;

$$\sigma\ (\bar{\nu}_e +^{37} Cl \rightarrow e^{-} +^{37} Ar) < 0.9x10^{-45} cm^2 \tag{1.14}$$

This result was the clue of that neutrinos and anti-neutrinos are different particles. Since the neutrinos used in this experiment came from the fission process it was anti-neutrinos. To be able to make this reaction occur one needed neutrinos. (Same method was used to detect solar neutrinos and since sun also emits neutrinos, the reaction observed. This will be mentioned in next section.)

To answer the question which reaction occurs and which do not " Lepton Number Conservation Rule" is assigned. According to this; for the leptons $(e^{-}, \mu^{-}, \tau^{-})$ lepton number +1 is assigned and for the anti-leptons $(e^{+}, \mu^{+}, \tau^{+})$ lepton number -1 is assigned. In an interaction this number must be conserved, like charge is conserved in an interaction. For instance;

$$\bar{\nu}_e + n \rightarrow p + e^{-} \tag{1.15}$$

interaction can not take place since the lepton number of the interaction particles is $L = -1$ (due to $\bar{\nu}_e$) however the lepton number of outgoing particles is $L = +1$ (due to electron). Instead of anti-neutrinos, if it were neutrinos, then the reaction would occur.

1.4.4 Discovery of Muon Neutrinos (ν_μ)

Cosmic rays are high energy particles coming from deep space. These rays are discovered in 1912 and can be thought as "natural accelerators". Since these rays enable to discover new particles and understand the nature of cosmic rays, it attracted scientists. In 1937, J.C Street and E.C Stevenson who were studying on cosmic rays discovered pion(π) which had a mass between electron and proton by using a cloud chamber [35]. They observed sometimes a positive and sometimes a negative particle. Therefore this was thought as the proposed particle of Yukawa which he proposed it to explain the nuclear forces that binds together the neutron and proton. Moreover, it is thought that decaying of Yukawa's particle should have similarities with β decay.

Using photographic emulsion technique, Carl D. Anderson and S.H. Neddermeyer designed an experiment at high altitudes. The purpose of choosing high mountains for the experiment was, atmosphere's preventing high energy particles from reaching its surface and also short life time of high energy particles. These particles decay before reaching the ground. Anderson and Neddermeyer observed a kink where π decayed. This was weird because it seemed momentum conservation is violated. Attempting a solution for this problem was easy when someone thinks about β decay. Neutrino should have been emitted in this decay and with this, momentum conservation rule was in safe again. Moreover, when tracking is analyzed, it is understood that the decayed particle was not an electron. It was heavier than electron. This is understood by looking at the brightness of the traces left in the film. This new particle was called as μ.

After the discovery of pion decay, $\pi \rightarrow \mu^- + \nu$ the question arose; Are the neutrinos emitted in pion decay were the same neutrinos as emitted in β decay or not ? In 1960, Pontecorvo [36] was so sure that they were different types of neutrino and even he named this new type neutrino as "neutrina", which means the feminine form of neutrino in Italian. Moreover, he suggested a method to observe it in a particle detector.

To be able to answer the question whether the neutrinos are same or not, an accelerator experiment is designed at Brookhaven National Laboratory. A proton beam is accelerated at 15 GeV and then hit a Be target which produced mostly pions (π^+ and π^-) and Kaons [37]. After a certain length of travel, pions and kaons decayed into muons and neutrinos. Then a

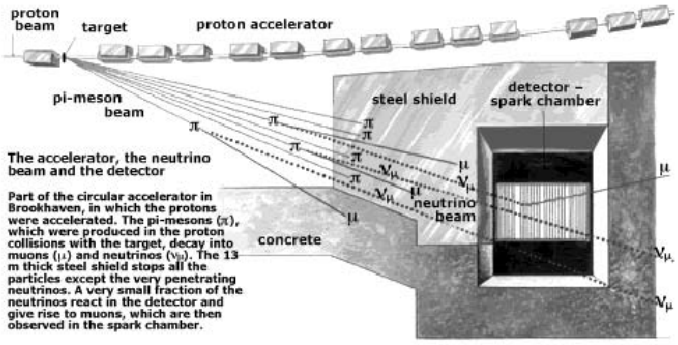

Figure 1.5: Schematic view of AGS neutrino experiment. (Adopted from [34].)

steel shielding is used to prevent charged and not highly penetrating particles, such as muons and pions to pass. Hence; with this shielding purely neutrino beam is acquired as shown in Figure 1.5. Then, this neutrino beam is passed through a spark chamber detector, which is made mostly of metal and used for detecting charged particles. To increase the interaction probability of neutrinos with matter, the mass of the target is increased by putting aluminum plates inside spark chamber. Therefore when neutrino interacted with matter there may have been four possible cases depending on the neutrino types or more clearly depending on the type of neutrinos in pion decay. These cases are;

$$\nu_\mu + n \rightarrow \mu^- + p$$

$$\bar{\nu}_\mu + p \rightarrow \mu^+ + n$$

and

$$\nu_\mu + n \rightarrow e^- + p$$

$$\bar{\nu}_\mu + p \rightarrow e^+ + n$$

It is expected that all the interactions take place if the neutrinos emitted from beta decay and pion decay were same. The tracking properties of electrons and muons are different in the sense that muons penetrate many layers of the spark chamber and leaves a long straight tracks, on the other hand electrons can not penetrate more than a few layers before forming an electromagnetic shower. As a consequence, when the data is analyzed only muon tracking was observed and no electrons which meant that the two neutrinos are different types. After this experiment, the neutrinos in β decay are called electron type neutrino(ν_e) and neutrinos emerging from pion decay are called muon type neutrinos (ν_μ).

By just conserving the charge and Lepton number conservation it is easy to understand which neutrino is antiparticle. With respect to this, pion decay should have been take place as

$$\pi^- \rightarrow \mu^- + \bar{\nu}_\mu$$

$$\pi^+ \rightarrow \mu^+ + \nu_\mu$$

so that lepton number is conserved in the interaction.

1.4.4.1 Muon Decaying to Neutrinos ($\mu \rightarrow e + 2\nu$)

In a similar way of detection of pion decay, muon decay is observed via photographic emulsion technique. There was a kink again. However, this time, assumption of existence of one neutrino was not enough to conserve momentum and energy. Because when the energy of emitted electron is measured, it is discovered that it was not a certain value (which meant it was not a two body decay) but varied in each measurement. Therefore, it is thought that in the decay of muon (at least) two neutrinos are emitted. Thus, the decay takes place as;

$$\mu^- \rightarrow e^- + \nu + \nu$$

However, since it was known that lepton number is conserved then one of the emitted neutrinos should have been anti-neutrino.

$$\mu^- \rightarrow e^- + \nu + \bar{\nu}$$

Unfortunately, it was not possible to decide of the neutrino types by just looking at the emulsion photographs. With the improvement of accelerator physics it became possible to produce and control high energy particles so that scientist could search so many channels. One of them was looking for the interaction of muon decaying into an electron and photon.

$$\mu^\pm \rightarrow e^\pm + \gamma$$

Surprisingly, this interaction has never been observed and has a branching ratio of Br ($\mu^+ \rightarrow e^+\gamma < 1.2x10^{-11}$) at 90% C.L [38]. As Richard Feynman said and became a rule of thumb in particle physics; "Whatever is not expressly forbidden is mandatory." [39] Therefore inspiring by lepton number conservation, electron and muon number conservation (after discovery of τ, tau number conservation also) is assigned too. Moreover, as shown in Table 1.1 there are

Table 1.1: Some selected experimental limits on lepton-number-violating processes. (Adopted from [34, 40].)

Process	Exp.limit on B R
$\mu \to e\gamma$	$< 1.2 \times 10^{-11}$
$\mu \to 3e$	$< 1.0 \times 10^{-12}$
$\mu(A,Z) \to e^-(A,Z)$	$< 6.1 \times 10^{-13}$
$\mu(A,Z) \to e^+(A,Z)$	$< 1.7 \times 10^{-12}$
$\tau \to \mu\gamma$	$< 1.1 \times 10^{-6}$
$\tau \to e\gamma$	$< 2.7 \times 10^{-6}$
$\tau \to 3e$	$< 2.9 \times 10^{-6}$
$\tau \to 3\mu$	$< 1.9 \times 10^{-6}$
$K^+ \to \pi^- e^+ e^+$	$< 6.4 \times 10^{-10}$
$K^+ \to \pi^- e^+ \mu^+$	$< 5.0 \times 10^{-10}$
$K^+ \to \pi^+ e^+ \mu^-$	$< 5.2 \times 10^{-10}$

so many interaction process which are not observed. In all these interactions lepton number conservation rule is violated.

With the assignment of new conservation rules; it is understood that the interactions of emitted neutrinos in muon decay are electron type anti-neutrino ($\bar{\nu}_e$) and muon type neutrino (ν_μ).

$$\mu^- \to e^- + \nu_\mu + \bar{\nu}_e$$

As a result, all three rules (conservation of lepton, electron and muon number) has been satisfied. Moreover, with these rules it became possible to determine which leptonic interactions could take place by just checking these rules.

1.4.5 Discovery of Tau Neutrino (ν_τ)

A third type of lepton, τ , which is much more heavier than electron and muon is discovered by experiments led by Martin Perl, who got the nobel prize in 1995 with this discovery. The search took three years, from 1974 to 1977 [41]. When τ is discovered, depending on the previous experiences it was thought that a third type of neutrino (ν_τ) should have existed too. An indirect evidence depended on the experiments of Z^0 boson decay [42] which is performed at Large Electron Positron Collider (LEP). A direct evidence result of the discovery was the observed interaction of $\nu_\tau + X \to \tau + Y$ in a similar way of muon neutrinos with DONUT (Direct Observation of Nu Tau) experiment at Fermilab in 2001. As shown in Table 1.1, also due to non existence of interactions like $\tau \to e + \gamma$ and $\tau \to \mu + \gamma$ tau number conservation

rule became necessary. With the discovery of third family of tau lepton and tau neutrino it is understood that three lepton family exists with the characteristic lepton numbers they have.

1.4.6 How Many Flavors of Neutrino Are There?

By measuring the total decay width, Γ_Z, of Z boson, it is possible to decide number of light neutrinos that is $m_\nu < m_Z/2$. With this method, if there exists heavier neutrinos ($m_\nu > m_Z/2$) we can not understand whether a fourth type of neutrino exists or not. For that, Large Hadron Collider (LHC) results should have been waited [1, 43]. Z boson can decay into hadrons ($\Gamma_{hadrons}$, that consists also $Z \rightarrow q + \bar{q}$), charged leptons ($\Gamma_{leptons}$, $Z \rightarrow l^+ + l^-$) and neutrinos ($\Gamma_{neutrinos}$, $Z \rightarrow \nu + \bar{\nu}$). Therefore the total width is equal to

$$\Gamma_Z = \Gamma_{hadrons} + 3\Gamma_{leptons} + N_\nu \Gamma_{neutrinos} \tag{1.16}$$

where factor 3 is due to three types of charged leptons that we already know and N_ν corresponds to number of neutrino flavors. These partial widths can be calculated using electroweak theory [39] and also can be measured experimentally. When all the experimental results are put in eqn 1.16, one gets $N_\nu = 2.9841 \pm 0.0083$ [34]. Moreover, as shown in Figure 1.6, Z resonance fits the data if the neutrino flavor type is three. The graph also shows the predicted results if $N_\nu = 2$ and $N_\nu = 4$.

1.5 Discovering and Understanding Neutrino Anomalies

1.5.1 Solar Neutrino Anomaly

Sun is the most powerful nuclear reactor in which thermonuclear reactions take place and it creates its energy via nuclear fusion. With fusion reactions, lighter elements such as hydrogen or helium constitutes heavier elements. According to Standard Solar Model (SSM), hydrogen and helium nuclei become so hotter due to immense gravitational pressure in the Sun's core so that they can fuse together. X-rays, γ rays and neutrinos are emitted in these fusion reactions. SSM predicts that most of the Sun's energy is produced due to proton proton(pp) cycle which means protons fuse together to form He nucleus. The pp chain is shown in Table 1.2. SSM prediction of neutrino energies are shown in every step [45].

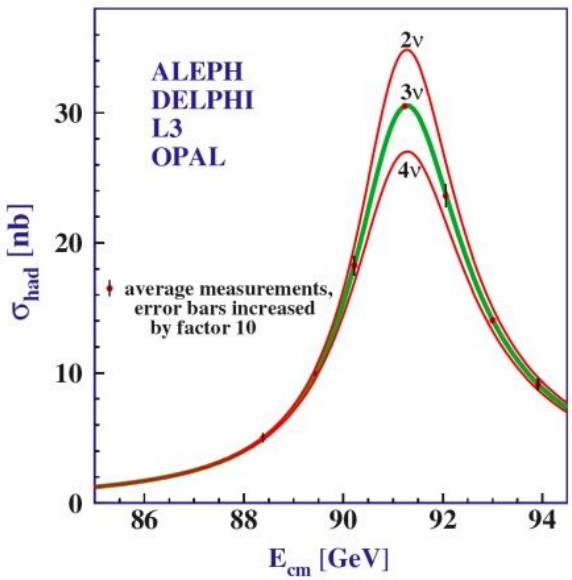

Figure 1.6: Cross section of the reaction $e^- + e^+ \rightarrow hadrons$ as a function of cm energy. The results belong to experiments ALEPH, DELPHI, L3 and OPAL. The red curves describes the Standard Model predictions for two and four light neutrino flavours. (Adopted from [44])

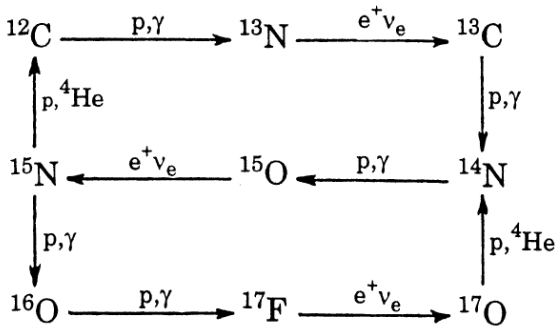

Figure 1.7: Schematic representation of CNO cyle. This also burns hydrogen to helium with C, N and O acting as catalysts and is responsible for 1.6% of the solar energy.(Adopted from [34])

Table 1.2: Nuclear reactions responsible for producing almost all of the Sun's energy and the different "types" of solar neutrinos (nomenclature): *pp*-neutrinos, *pep*-neutrinos, *hep*-neutrinos, ^{7}Be-neutrinos, and ^{8}B-neutrinos. 'Termination' refers to the fraction of interacting protons that participate in the process. (Adopted from [17, 45].)

Reaction	Termination (%)	Neutrino Energy (MeV)	Nomenclature
$p + p \rightarrow {}^2\mathrm{H} + e^+ + \nu_e$	99.96	< 0.423	*pp*-neutrinos
$p + e^- + p \rightarrow {}^2\mathrm{H} + \nu_e$	0.044	1.445	*pep*-neutrinos
${}^2\mathrm{H} + p \rightarrow {}^3\mathrm{He} + \gamma$	100	–	–
${}^3\mathrm{He} + {}^3\mathrm{He} \rightarrow {}^4\mathrm{He} + p + p$	85	–	–
${}^3\mathrm{He} + {}^4\mathrm{He} \rightarrow {}^7\mathrm{Be} + \gamma$	15	–	–
${}^7\mathrm{Be} + e^- \rightarrow {}^7\mathrm{Li} + \nu_e$	15	0.863(90%) 0.386(10%)	^{7}Be-neutrinos
${}^7\mathrm{Li} + p \rightarrow {}^4\mathrm{He} + {}^4\mathrm{He}$		–	–
${}^7\mathrm{Be} + p \rightarrow {}^8\mathrm{B} + \gamma$	0.02	–	–
${}^8\mathrm{B} \rightarrow {}^8\mathrm{Be}^* + e^+ + \nu_e$		< 15	^{8}B-neutrinos
${}^8\mathrm{Be} \rightarrow {}^4\mathrm{He} + {}^4\mathrm{He}$		–	–
${}^3\mathrm{He} + p \rightarrow {}^4\mathrm{He} + e^+ + \nu_e$	0.00003	< 18.8	*hep*-neutrinos

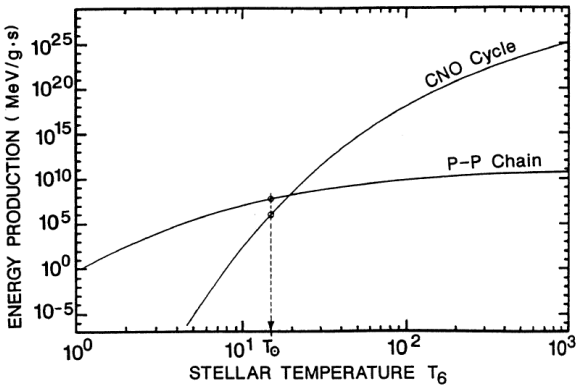

Figure 1.8: Contributions of the CNO cyle and pp chain for energy production in stars as a function of the central temperature. (Adopted from [34])

Another way that Sun creates its energy is CNO (Carbon,Nitrogen,Oxygen) cycle [46, 47] in which hydrogen is burnt into Helium as shown in Figure 1.7. CNO cycle forms % 1.6 of Solar energy. In Figure 1.8 , the contributions of pp and CNO cycle to energy production in stars as a function of the central temperature is shown. CNO cycle becomes dominant above 20 million degrees [48] thus, in sun pp cycle is dominant.

Detection of the neutrinos emitted in fusion reactions in pp cycle was important to be able to understand the neutrino interactions better and to test Standard Solar Model. The reason that Ray Davis could not observe neutrinos via interaction, $\nu +^{37} Cl \rightarrow e^{-} +^{37} Ar$, was thought that he performed his experiment near nuclear reactors in which the source was anti-neutrinos. This interaction violated lepton number conservation. However, if the same experimental method is used to detect the solar neutrinos emitted via fusion reactions in pp cycle , it is thought that the interaction would be observed.

To be able to decrease the background effects, the experiment is set up underground in the Homestake gold mine of South-Dakota in 1964. They tried to observe the neutrinos emitted from the decay of ^{8}B (Boron-8) since this decay channel has the highest energy and therefore is easy to detect. Ray Davis managed to observe and measured the flux of solar neutrinos and awarded with the Nobel prize in 2002 “for pioneering contributions to astrophysics, in particular for the detection of cosmic neutrinos.”

To compare the experimental results with the SSM prediction one needed to calculate the solar neutrino flux. This flux is calculated by theoreticians [49]. Taking into account the SSM

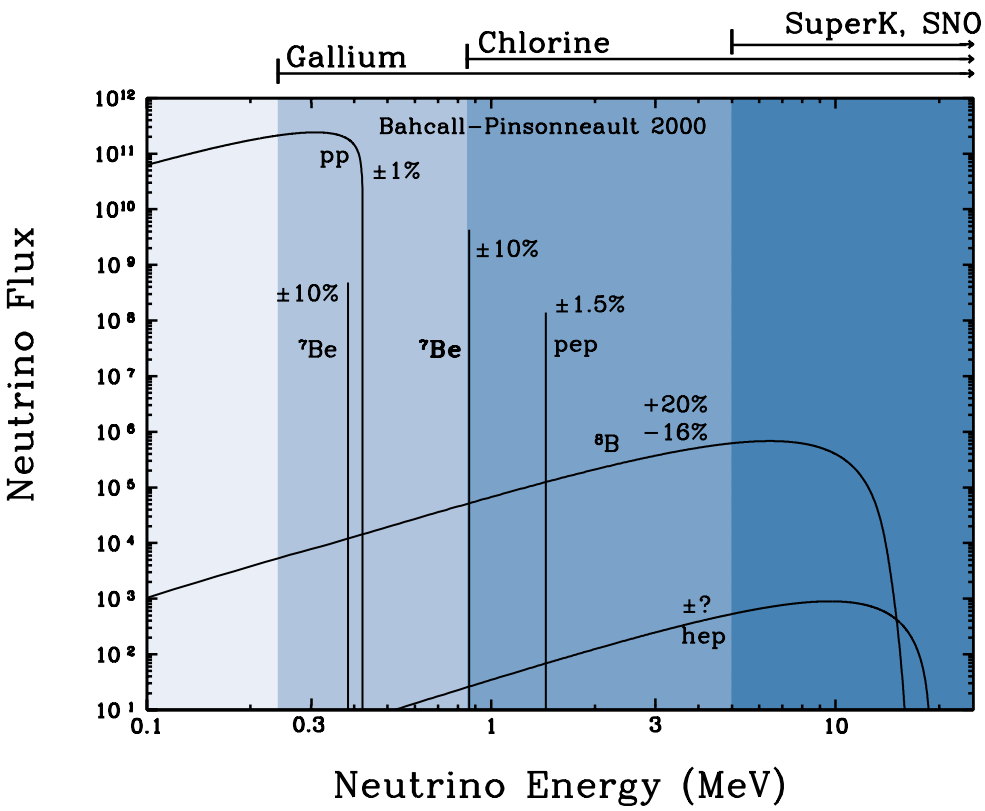

Figure 1.9: The predicted solar neutrino energy spectrum. The figure shows the energy spectrum of solar neutrinos predicted by the most recent version of the standard solar model. For continuum sources, the neutrino fluxes are given in number of neutrinos $cm^{-2}s^{-1}$ MeV^{-1} at the Earth's surface. For line sources, the units are number of neutrinos $cm^{-2}s^{-1}$. Total theoretical uncertainties are shown for each source. (Adopted from [17].)

neutrino flux calculation, Davis group expected to see one solar neutrino event depending on their experimental configuration. However, what they observed was one fourth the expected one. The first solutions that came to mind are;

- The experiment was not good enough to count the neutrino rate.
- Standard Solar Model is not successful enough
- Neutrinos have some unknown interactions or properties

Homestake experiment took its first data in 1968 and continued taking data for over thirty years. To confirm the Homestake experiment results and also check the first solution is correct or not, in 1985, Kamiokande experiment, which is a very large water cherenkov experiment, started. The idea was to look for proton decay, $p \rightarrow e^+ + \pi^0$ and to be able to detect solar

neutrinos via neutrino electron scattering, $\nu_e + e^- \rightarrow \nu_e + e^-$. This japanese experiment was only sensitive to high energy neutrinos emitted from Sun, which is Boron-8 chain. When neutrino interacted with electron, electron is recoiled and then cherenkov light is emitted. With this information electron energy and direction could be measured which meant also neutrino energy and direction could be measured. The results were confirming Homestake experiment and were contradicting with SSM as [22]

$$\frac{\Phi_{8experiment}}{\Phi_{8SSM}} \approx 0.47 \pm 0.10\ (1\sigma) \tag{1.17}$$

where Φ_8 refers to neutrino flux coming from ^8B decay. Both Homestake and Kamiokande experiments were not sensitive to neutrinos emitted from pp cycle. To detect these neutrinos Gallium(Ga) is used as a target [50]. This method is used by the experiments the GALLEX (Italy) which started in 1991 and SAGE (Soviet American Colloboration) which started in 1990. The reaction to be searched was $^{71}Ga + \nu_e \rightarrow^{71} Ge + e^-$ with a threshold energy of 233 keV. Similar to Homestake experiment, chemical techniques were used to isolate and count number of Ge atoms. The experimental result was ; $77.5 \pm 6.2(stat)^{4.3}_{-4.7}(sys)\ SNU$. On the other hand theoretical prediction of SSM was 128±8 SNU [51, 52] where SNU (solar neutrino unit) is equal to $1SNU = 10^{-36}$ captures per target atom per second. All three experiments had its own characteristic properties and advantages. Kamiokande experiment was able to measure neutrino energy and correlate the incoming neutrino direction with respect to sun position. However it was only sensitive to ^8B neutrinos. Although radiochemical experiments (Gallex, SAGE, Homestake) could not measure the energy of neutrinos they were sensitive to lower energy neutrinos emitted from sun. The Figure 1.9 shows also the sensitivity of experiments to neutrino energies.

All these experiments results with the results of Kamland, Superkamiokande and Sudbury Neutrino Observatory(SNO) claimed that the observed neutrino flux is less than the SSM prediction and this unexplained phenomena is named as Solar Neutrino Anomaly. Figure 1.10 shows the comparison of the solar neutrino flux measured by experiments with the SSM predictions. This made the astrophysicists to reconsider SSM again, on the other hand, made particle physicists to think about neutrino interactions again.

Sudbury Neutrino Observatory (SNO) is located about 2 km underground in Canada which uses heavy water to detect solar neutrinos from Boron-8. The interactions searched were;

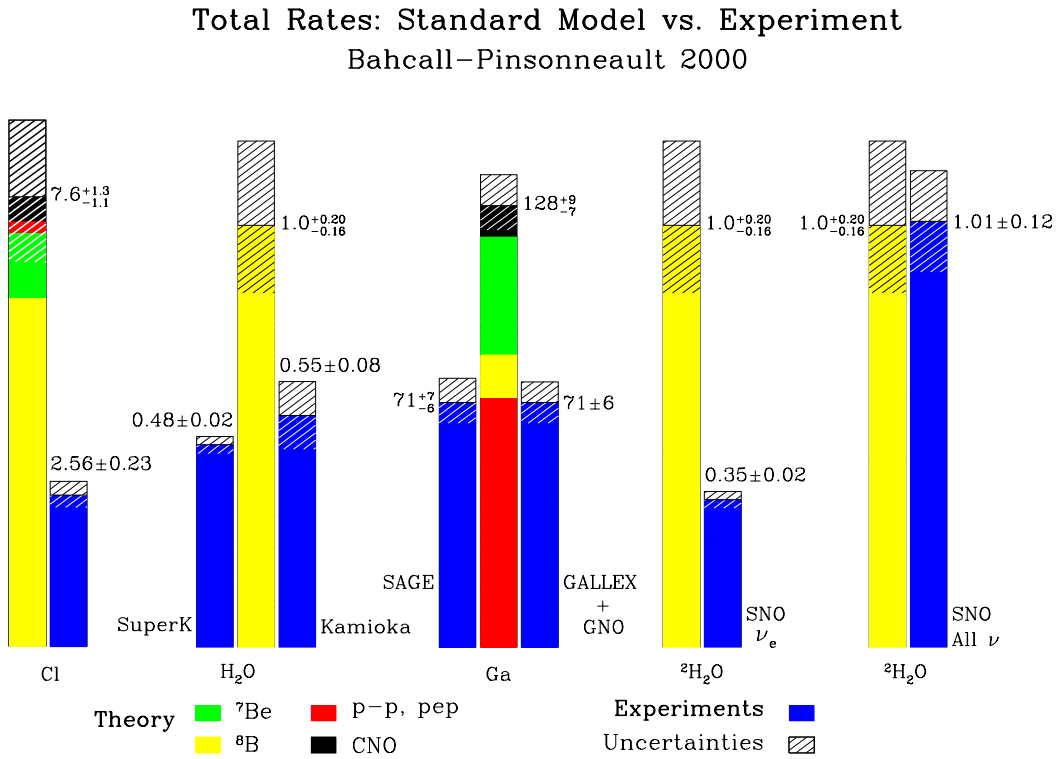

Figure 1.10: Predictions of the standard solar model and the total observed rates in the six solar neutrino experiments: chlorine, SuperKamiokande, Kamiokande, GALLEX, SAGE, and SNO. The model predictions are color coded with different colors for the different predicted neutrino components. For both the experimental values and the predictions, the 1 sigma uncertainties are indicated by cross hatching.(Adopted from [17].)

$$\nu +^2 H \rightarrow p + p + e^-$$

$$\nu + e^- \rightarrow \nu + e^-$$

$$\nu +^2 H \rightarrow \nu + p + n$$

For the first interaction the observed particle was e^- in the experiment and this interaction can only take place if the neutrino is electron type. However, the second interaction which is a neutrino electron scattering process, can take place via all type of neutrinos. This interaction is searched in Superkamiokande either. The neutrinos are mostly electron type neutrinos ($\%85\nu_e, \%15\nu_\mu, \nu_\tau$) [17] in the energy range considered. The electrons both observed in Deutron interaction and electron scattering are separated each other by the help of kinematics of different interactions. The third interaction is detected via emitted photons after neutron

capture in deutron and chlorine. This last interaction also can take place via all neutrino types and enable SNO to observe the total flux of neutrinos. SNO is important in the sense that it exactly showed that muon type and tau type neutrinos are coming from the sun [53].

1.5.2 Atmospheric Neutrino Anomaly

Cosmic rays are constituted of about %98 hadrons and %2 electrons. Protons dominate (%87) the hadronic part. When cosmic rays hit the atmosphere, a shower of mesons are created. With the decay of mesons, muons and muon type of neutrinos are created and these muons decay into neutrinos. All these neutrinos emerging with the interaction of cosmic rays with the atmosphere are called atmospheric neutrinos. The dominant part of the decay chain is consisted of pions and Kaons.

$$\pi^+ \rightarrow \mu^+ + \nu_\mu$$

$$\pi^- \rightarrow \mu^- + \bar{\nu_\mu}$$

$$\mu^+ \rightarrow e^+ + \nu_e + \bar{\nu}_\mu$$

$$\mu^- \rightarrow e^- + \bar{\nu}_e + \nu_\mu$$

and

$$K^\pm \rightarrow \mu^\pm + \nu_\mu(\bar{\nu}_\mu)$$

$$K_L \rightarrow \pi^\pm + e^\pm + \nu_e(\bar{\nu}_e)$$

For the energetic neutrinos ($E_\nu \approx 1$ GeV) the last decay channel, $K_L \rightarrow \pi \pm +e^\pm + \nu_e(\bar{\nu}_e)$, is the most dominated. Therefore, for low neutrino energies the ratio of the flux of muon neutrino to electron neutrino is expected to be 2. Muon neutrinos are emerging from both pion and muon decay, on the other hand electron neutrinos are created only from muon decay. When the energy of muon increases then the fraction of muons that decays in flight decreases. Because in this case Lorentz boost for muons is high enough to reach the earth surface. Since the decaying number of muon decreases, electron neutrinos are not created and the ratio of muon neutrinos to electron neutrinos are expected to be larger than 2. Although theoretical calculation of the flux of atmospheric neutrinos and detection of them was too hard, it was possible to measure this ratio of the flux of two types.

NUSEX, Frejus, Soudan, Macro, Kamiokande and IMB were the experiments searching for atmospheric neutrinos. The first two of them were water cherenkov experiments and the rest

Table 1.3: Summary of R measurements.([17, 54])

Experiment	kt-yr	events	R (data/MC)	"material"
IMB	7.7	610	$0.54 \pm .05 \pm .11$	water
Kamiokande	7.7	482	$0.60^{+.06}_{-.05} \pm .05$	water
Soudan-2	3.2	~200	$0.61 \pm .15 \pm^{\cdot} 05$	iron
Fréjus	2.0	200	$1.00 \pm .15 \pm .08$	iron
NUSEX	0.7	50	$0.96^{+.32}_{-.28}$	iron

was calorimeter like detectors. The results of the experiments are given in Table 1.3 and [54], where $R = \frac{[N(\mu-like)/N(e-like)]_{obs}}{[N(\mu-like)/N(e-like)]_{exp}}$. Ignoring the result of Soudan experiment, it seemed that cherenkov experiments measure the value R smaller than 1, on the other hand calorimeter like experiments measured R around 1. R values being smaller than 1 indicates that ν_μ flux is less than the expected.

Kamiokande experiment was able to give information about the neutrino directions also. Therefore, electron and muon type of neutrino flux can be measured as a fraction of neutrino direction. It is observed that, muon type of neutrino flux was larger from above than below on the other hand electron type of neutrino flux was not changing [55].

Super Kamiokande is a developed version of Kamiokande designed to improve the sensitivity of measurement of proton decay, to check atmospheric anomaly and to enhance the measurements on ^8B solar neutrino spectrum. Super Kamiokande showed that without any doubt muon type atmospheric neutrinos disappeared which is called as atmospheric neutrino anomaly [56]. Moreover, they showed that disappearance rate is related with neutrino energy and baseline.

1.5.3 Neutrino Oscillations

To explain the atmospheric and solar neutrino anomalies, it was believed that Standard Model (SM) is not fully correct in description of neutrino production, propagation or in detection. There were some ideas to solve these anomalies. One of the possible explanation was neutrinos having a lifetime which means also neutrinos should be massive. If this is the case neutrinos could decay into either other SM particles or into new lighter particles. If this idea was correct, it could be a solution to both atmospheric and solar neutrino anomaly. The disappearance of electron type neutrinos and muon type neutrinos could be explained as decaying

into new particles. This solution lost its reliability after the measurement of mass of ν_e as $m^2_{\nu_e} < 5eV^2$ so that they could not decay into new particles. Another solution candidate was the following ; The weak interaction was wrong and neutrinos are absorbed much more than predicted while traversing the matter. However in reactor neutrino experiments and accelerator experiments the result fitted well with the theory therefore this solution is ignored too.

Another solution to solar neutrino anomaly might be neutrinos having magnetic moments. If this is the case, when there is intense magnetic fields, neutrinos could be converted into either anti-neutrinos or right handed neutrinos by emitting a photon [17]. Homestake and Gallium experiments can only detect neutrinos. If neutrinos are converted into anti-neutrinos this could explain the solar neutrino deficit. However, up to now experiments could only put bounds for the magnetic moment as $\mu_{\bar{\nu}_e} < 7.4 \times 10^{-4}\, \mu_B$ at 90% Cl [62].

The other alternative which mimics also neutrinos being massive is neutrinos changing flavor while oscillating. This model is a candidate to answer both solar and atmospheric anomalies. Neutrinos created in one flavor ν_α, could convert into another neutrino ν_β, while traveling. The probability of neutrinos changing flavor depends on the distance traveled and energy of neutrinos. This solution which will be explained in more detail in the following section is the accepted solution.

1.5.3.1 Neutrino Oscillations in Vacuum[1]

If each of the neutrinos and each of the leptons have different masses, then it is possible to consider lepton mixing. Since neutrinos are massive, there may have mass eigenstates (ν_i, where $i = 1, 2, 3....$ and each with a mass m_i) of neutrinos which may differ from the flavor eigenstates.

To explain the lepton mixing, consider the decay of $W^+ \rightarrow \nu_i + \bar{l}_\alpha$ where α corresponds to e, μ or τ. Although the created lepton is one flavor, the emitted neutrino does not always have the same mass eigenstate. Amplitude, creating the specific combination of $\bar{l}_\alpha + \nu_i$, is denoted by $U^*_{\alpha i}$. Then flavor eigenstate can be written in mass eigenstates as;

$$|\nu_\alpha >= \sum_i U^*_{\alpha i} |\nu_i > \tag{1.18}$$

[1] For this subsection most of the materials was obtained from ref [57]

$U^*_{\alpha i}$ matrix is named as Maki-Nagakawa-Sakata-Pontecorvo (MNSP) lepton mixing matrix. So each mass eigenstate can be represented in neutrino flavors as;

$$|\nu_i >= \sum_i U_{\alpha i}|\nu_\alpha > \tag{1.19}$$

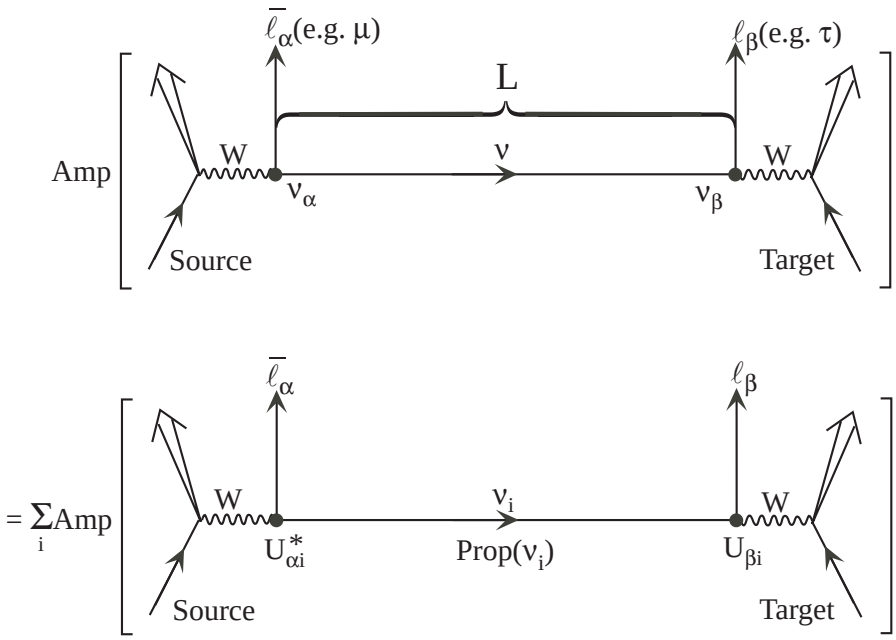

Figure 1.11: Neutrino flavor change (oscillation) in vacuum. "Amp" denotes an amplitude.(Taken from [57])

The situation of neutrino oscillations in vacuum is shown in Figure 1.11. Via weak interaction, neutrino flavor (ν_α) and a charged lepton $\bar{l}_\alpha$ is created. Thus, the initial neutrinos are α types. After a distance, L, traveled, α type neutrinos change into β type and interacts with the target and produces a charged lepton l_β. The upper line of the figure shows this interaction and in bottom line the probability amplitude of this interaction is schematically shown. Since ν_α is a superposition of mass eigenstates, with the creation in the source, it can be in any of the mass eigenstate ν_i. This amplitude is $U^*_{\alpha i}$. Therefore, different probabilities of different mas eigenstates should be taken into account. One more probability calculation needs to be done while neutrinos propagating from source to target. This amplitude is denoted as Prop(ν_i) in the Figure. And final probability factor is due to the amplitude for the charged lepton created by the ν_i when interacted with the detector. Due to Hermiticity, this amplitude becomes $U_{\beta i}$.

Therefore from source to target the amplitude becomes ;

$$\mathrm{Amp}(\nu_\alpha \to \nu_\beta) = \sum_i U^*_{\alpha i}\mathrm{Prop}(\nu_i)U_{\beta i} \ . \tag{1.20}$$

Now the question becomes to determine Prop(ν_i). In the rest frame of mass eigenstate, ν_i, the time is denoted as τ. Then state vectors obey the Schrodinger equation (taking $\hbar = 1$ and $c = 1$) as;

$$i\frac{\partial\psi}{\partial t} = E\psi \tag{1.21}$$

$$i\frac{\partial}{\partial\tau_i}|\nu_i(\tau_i) > = m_i|\nu_i(\tau_i) > \ . \tag{1.22}$$

where the energy of ν_i is only rest mass energy since we are in the rest frame of ν_i. Then solution becomes;

$$|\nu_i(\tau_i) > = e^{-im_i\tau_i}|\nu_i(0) > \tag{1.23}$$

With this, Prop(ν_i) has been acquired where τ is the proper time. However, what we need is the situation in lab frame. Because, the measurable quantities are the distance "L", from source to detector and the time "t" between the neutrino is created from source and detected via detector with respect to lab frame. To define the amplitude of Prop(ν_i) we need to define it in lab frame. For this the phase, $m_i\tau_i$ becomes by Lorentz invariance

$$m_i\tau_i = E_i t - p_i L \ . \tag{1.24}$$

Momentum of the mass eigenstate become in the ultra relativistic region (E$\gg m\nu_i$)

$$E_i^2 - p_i^2 = m_i^2 \tag{1.25}$$

then

$$p_i = \sqrt{E^2 - m_i^2} \cong E - \frac{m_i^2}{2E} \ . \tag{1.26}$$

Thus, $m_i\tau_i$ takes the form in lab frame as;

$$m_i\tau_i \cong E(t - L) + \frac{m_i^2}{2E}L \ . \tag{1.27}$$

The phase $E(t-L)$ can be ignored since it is common to all interfering mass eigenstates [57]. Hence we get,

$$\mathrm{Prop}(\nu_i) = \exp[-im_i^2 \frac{L}{2E}] \ . \tag{1.28}$$

Then the amplitude in equation 1.20 becomes as;

$$\mathrm{Amp}(\nu_\alpha \to \nu_\beta) = \sum_i U^*_{\alpha i} e^{-im_i^2 \frac{L}{2E}} U_{\beta i} \ . \tag{1.29}$$

This equation is valid for any number of mass eigenstates and any number of flavors. To find the oscillation probability we need to square the amplitude and by using the unitarity of the matrix U we get;

$$\begin{aligned} \mathrm{P}(\nu_\alpha \to \nu_\beta) &= |\mathrm{Amp}(\nu_\alpha \to \nu_\beta)|^2 \\ &= \delta_{\alpha\beta} - 4\sum_{i>j} \Re(U^*_{\alpha i} U_{\beta i} U_{\alpha j} U^*_{\beta j}) \sin^2(\Delta m^2_{ij} \frac{L}{4E}) \\ &\quad + 2\sum_{i>j} \Im(U^*_{\alpha i} U_{\beta i} U_{\alpha j} U^*_{\beta j}) \sin(\Delta m^2_{ij} \frac{L}{2E}) \ , \end{aligned} \tag{1.30}$$

where

$$\Delta m^2_{ij} \equiv m_i^2 - m_j^2 \ . \tag{1.31}$$

It is important to note that, although there are only three type of neutrino flavors there may have been more than three mass eigenstates. The reason that we have not observed all the linear combination of mass eigenstates could be not having a weak eigenstate partner of the some linear combinations of the mass eigenstates. This means some linear combinations may not couple to $W^\pm$ or Z bosons. Such neutrinos not having weak couplings is called sterile neutrinos and trying to be observed in experiments [58].

To find the oscillation between anti-neutrino we can assume that CPT invariance holds. Then;

$$\mathrm{P}(\bar{\nu_\alpha} \to \bar{\nu_\beta}) = \mathrm{P}(\nu_\beta \to \nu_\alpha) \ . \tag{1.32}$$

from equation 1.30;

$$P(\nu_\beta \to \nu_\alpha;\ U) = \mathrm{P}(\nu_\alpha \to \nu_\beta;\ U^*) \ . \tag{1.33}$$

and [57]

$$\begin{aligned} P(\bar{\nu_\alpha} \to \bar{\nu_\beta}) &= \delta_{\alpha\beta} - 4\sum_{i>j} \Re(U^*_{\alpha i}U_{\beta i}U_{\alpha j}U^*_{\beta j})\sin^2(\Delta m^2_{ij}\frac{L}{4E}) \\ & \quad 2\sum_{i>j} \Im(U^*_{\alpha i}U_{\beta i}U_{\alpha j}U^*_{\beta j})\sin(\Delta m^2_{ij}\frac{L}{2E}) \ . \end{aligned} \tag{1.34}$$

As seen in the oscillation probability formula, if neutrinos are massless, then all $\Delta m^2_{ij} = 0$, so oscillation probability becomes $P(\overset{(-)}{\nu_\alpha} \to \overset{(-)}{\nu_\beta}) = \delta_{\alpha\beta}$. Hence flavor changing process does not occur. This is the reason why neutrino oscillations imply neutrinos being massive. The reason for neutrino oscillation implying lepton mixing is this; if we assume flavor eigenstate and mass eigenstate is same , in other words in a decay of $W^+ \to \bar{l}_\alpha + \nu_i$, the same lepton is occurred via the same neutrino mass eigenstate. That is, if $U^*_{\alpha i} \neq 0$ then $U_{\alpha j}$ must be equal to zero for $j \neq i$. In that case the probability equation becomes $P(\overset{(-)}{\nu_\alpha} \to \overset{(-)}{\nu_\beta}) = \delta_{\alpha\beta}$. Therefore to talk about neutrino oscillations, lepton mixing should exist.

When the dimensional parameters are added we get the oscillation parameters as;

$$\Delta m^2_{ij}\frac{L}{4E} = 1.27\,\Delta m^2_{ij}(\mathrm{eV}^2)\frac{L\,(\mathrm{km})}{E\,(\mathrm{GeV})} \ . \tag{1.35}$$

Therefore as it is seen from this equation, the probability of flavor changing interactions depends on the parameter L/E. From oscillation experiments one can not decide neutrino masses, can only get information about the mass differences.

1.5.3.2 Neutrino Oscillations With Two Flavors

The two neutrino oscillation case is generally enough to explain the experimental results. In this case assuming there are only two mass eigenstates (ν_1 and ν_2) and two corresponding flavor eigenstates (ν_e and ν_μ) will be enough to search neutrino oscillations. In this case mass splitting will be equal to $\Delta m^2 = m^2_\mu - m^2_e$. Mixing matrix can be taken as;

$$U = \begin{array}{c} \\ \nu_e \\ \nu_\mu \end{array} \begin{array}{c} \begin{array}{cc} \nu_1 & \nu_2 \end{array} \\ \begin{bmatrix} \cos\theta & \sin\theta \\ -\sin\theta & \cos\theta \end{bmatrix} \end{array} \ . \tag{1.36}$$

Therefore

$$|\nu_e >= \cos\theta|\nu_1 > + \sin\theta|\nu_2 > \tag{1.37}$$

$$|\nu_\mu >= -\sin\theta|\nu_1 > +\cos\theta|\nu_2 > \tag{1.38}$$

Then probability equation given in equation 1.30 turns into;

$$P(\nu_e \to \nu_\mu) = P(\nu_\mu \to \nu_e) = P(\bar{\nu}_e \to \bar{\nu}_\mu) = P(\bar{\nu}_\mu \to \bar{\nu}_e) = \sin^2 2\theta \sin^2(\Delta m^2 \frac{L}{4E}) \tag{1.39}$$

In an experiment when the distance L and E is controllable then the unknown parameters become the mixing angle θ and mass differences Δm.

There are two possible ways to search neutrino oscillations. One of them is the disappearance experiment. Starting the experiment with a known flux of ν_α and observing the decreased flux due to oscillation to other types one can decide the oscillation parameters. With disappearance experiments, it is impossible to detect new type of neutrinos. The other way is the appearance experiment. In this case, starting with a known flux and type of ν_α, other type of neutrinos, ν_β, which are emerged due to oscillations is trying to be detected.

Neutrino oscillations can be searched via so many experimental setups which are designed for detecting solar, atmospheric or reactor neutrinos depending on the appearance or disappearance method. As seen from the probability formula 1.39, depending on the relation between L/E and Δm^2 the specialized experiments have their own advantages and disadvantages. Transition probabilities depend on the parameters of L/E . According to this [34];

If $L/E \ll \frac{4}{\Delta m^2}$ then, there is not enough time for neutrinos to oscillate.

If $L/E \gtrsim \frac{4}{\Delta m^2}$ then, this is the most sensitive region to observe oscillation and

If $L/E \gg \frac{4}{\Delta m^2}$ then, many oscillations take place between the source and detector. Hence, in this case, generally the average transition probability could be measured.

Therefore each type of experiments has its own range for the oscillation parameters (Δm and θ). For instance one can not compare accelerator experiment results for which $E \approx 1-100$ GeV and $L \approx 1$ km , with solar neutrino detection experiment for which $E \approx 1$ MeV and $L \approx 10^8$ km.

Using the reactors and accelerator as neutrino sources and building detectors by arranging the distance "L" between source and detector is a way to detect oscillations. There are many experiments designed to detect neutrino oscillations [34]. The present situation and allowed regions for the oscillation parameters are shown in Figure 1.12.

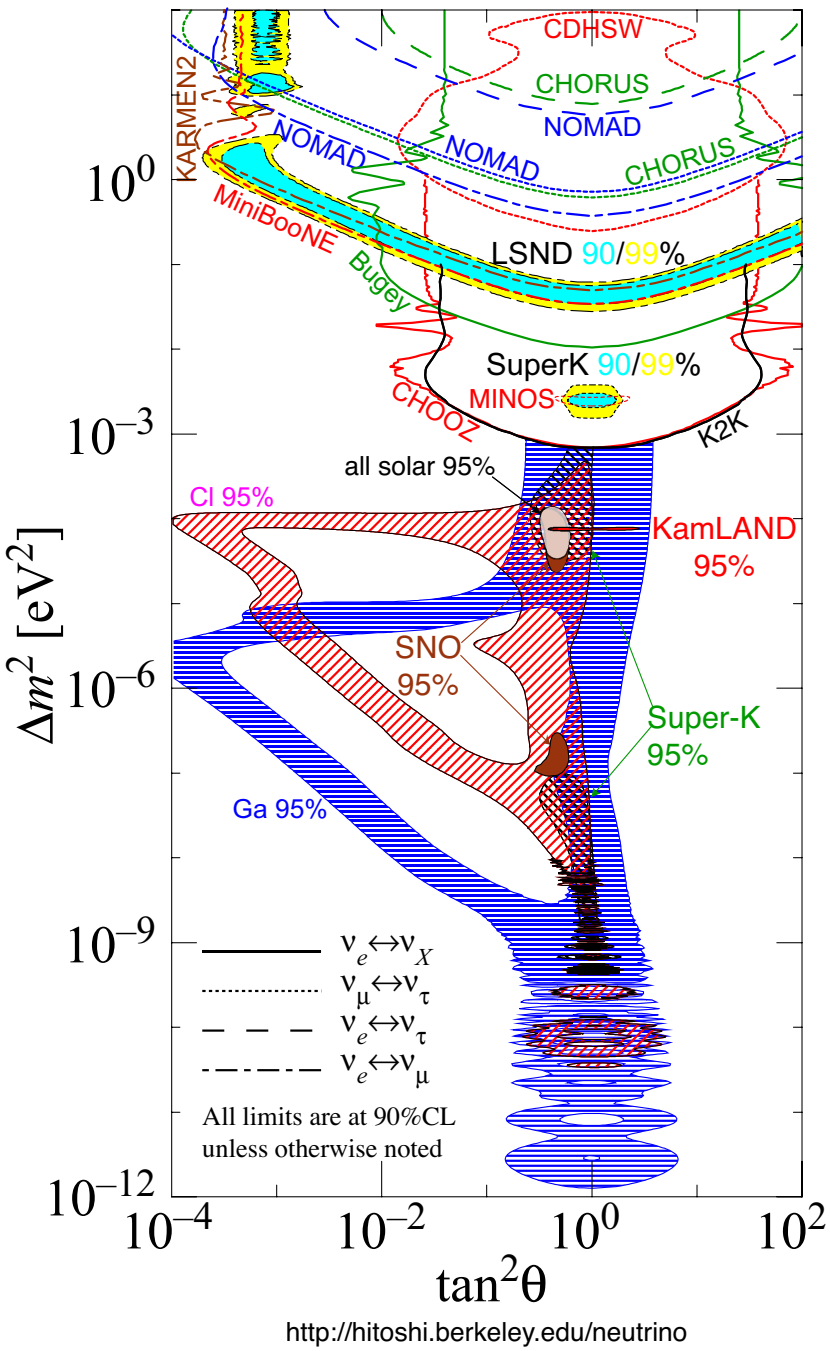

Figure 1.12: Present situation of oscillation parameters.

When neutrinos travel from the source to detector it does not travel in a vacuum but through earth matter. While neutrinos are traveling there may have coherent scattering with the particles they encounter and this can not be neglected. This effect is known as Mikheyev-Smirnov-Wolfenstein (MSW) effect. For details see [34, 57]

CHAPTER 2

TEXONO EXPERIMENT

Taiwan EXperiment On NeutrinO (TEXONO) collaboration was established in 1997 among scientists from Taiwan and China to conduct an experimental research in neutrino and astroparticle physics[59]. With the participation of the institutes from Turkey (METU in 2004), India (BHU) and USA (University of Maryland) the collaboration enlarged.

The research program is mainly related with the low energy low background experiments by using detectors with high atomic mass nuclei such as solid state device and scintillating crystals to search neutrino properties and interactions in low energy region. Texono is a reactor neutrino experiment which is located near a nuclear power station which has the benefit of high anti-neutrino flux. With three different experimental set up (1.06 kg HPGe, 4×5 g ULEGe and CsI (Tl) scintillating crystal detector) data is taken and with these data, neutrino magnetic moment, Weinberg angle measurements and cold dark matter, axions, Non-Standard Interaction of neutrinos and Unparticle physics search are conducted [6, 60, 61, 62, 63].

In the following sections, first, information about the Kuo-Sheng Neutrino Laboratory(KSNL) is given, then a brief description for the detectors; ULB-HP-Ge detectors and CsI (Tl) scintillating crystals is given, respectively.

2.1 Kuo-Sheng Neutrino Laboratory

KSNL is located at a distance of 28 m from the reactor core of "Kuo-Sheng Nuclear Power Station (KSNPS)" which has 2.9 GW nominal thermal output. The total anti-neutrino flux is around $6.4\times10^{12}\ cm^{-2}\ s^{-1}$. The schematic view of nuclear power plant is shown in Figure 2.1. Experimental set-up is placed 12 m below sea level. The inner target volume has the dimen-

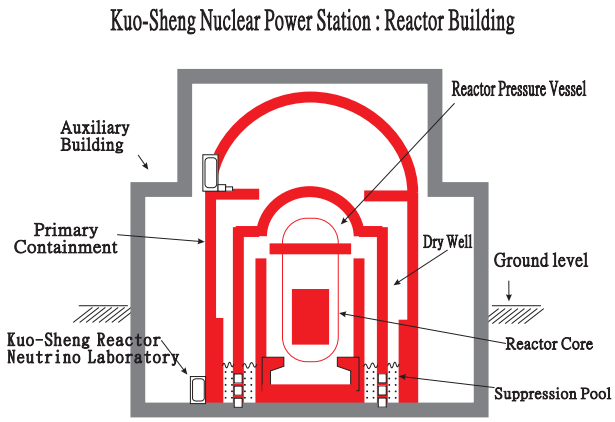

Figure 2.1: Schematic layout of the Kuo-Sheng Neutrino Laboratory together with the reactor core and building. (Adopted from [61].)

sion of 100 cm x 180 cm x 75 cm and this space enabled to place different detectors (both Ultra Low Background High Purity Ge (ULB-HPGe) and CsI (Tl) scintillating crystal detectors) at the same time. This place is covered by 4π passive shielding materials which weighs totally 50 tons. These shielding materials include, as shown also in Figure 2.2, from outside to inside; 2.5 cm thick plastic scintillator panels with photomultiplier tubes at both ends which is used for cosmic ray veto (CRV), 15 cm of lead and 5 cm of stainless steel support structures which is used for suppressing the ambient radioactivity, 25 cm of boron loaded polyethylene which is used to absorb mostly cosmic induced neutrons which are slowed down by lead and steel, and 5 cm of Oxygen-Free-High-Conductivity (OFHC) copper which suppress residual radioactivity from the shielding materials itself. To be able to prevent background events due to the diffusion of the radioactive radon gas, the inner target detectors are covered by a plastic bag flushed with dry nitrogen.

The reactor functions 18 months continually in normal conditions and Reactor is in OFF period around 50 days and in this period, one third of the fuel elements is replaced. Reactor ON/OFF data taking process has been started in July 2001 with 1.06 kg of ULB-HP Ge detector. In 2003, 186 kg of CsI (Tl) crystal scintillators are added near ULB-HP Ge detectors and both detectors started to take data in parallel with same data acquisition system but with different trigger systems. Data taking with ULB-HP Ge detector continued up to October 2005 and then replaced with 4×5 gr ULB-HP Ge detector to search Dark matter [6] and ν-Nucleus coherent scattering [64]. The data taking periods with CsI (Tl) and Ge detectors are shown in Table 2.1 and 2.2. These tables show the data analyzed in order to search neutrino

magnetic moment and neutrino electron cross section measurement in low energy.

Table 2.1: Summary of the key information on the three data taking periods with 1.06 kg HPGe detector which is used for neutrino magnetic moment search. (Adopted from [62]).

Period	Data Taking Calendar Time	Reactor ON Real Time (days)	Reactor ON Live Time (days)	Reactor OFF Real Time (days)	Reactor OFF Live Time (days)	DAQ Live Time (%)	Average $\bar{\nu}_e$ flux (10^{12} cm^{-2}s^{-1})
I	July 2001 - April 2002	188.2	180.1	55.1	52.7	95.7	6.29
II	Sept. 2002 - April 2003	125.8	111.7	34.4	31.5	89.4	6.53
III	Sept. 2004 - Oct. 2005	303.9	278.9	48.7	43.6	91.5	6.51
Total	–	617.9	570.7	138.2	127.8	92.4	6.44

2.2 ULB-HP Ge DETECTOR

The schematic view of experimental set-up is shown in Figure 2.3. The detector is surrounded by NaI (Tl) and CsI (Tl) crystal scintillators which function as anti-Compton veto (ACV) detector. This CsI (Tl) scintillators is coupled to 12 cm Photo Multiplier Tube (PMT). There is a 4 cm thick CsI (Tl) "base-detector" at the bottom and 5 cm thickness of Na (Tl) "ring detector" on the two sides of the cryostat. This whole set-up is covered by 3.7 cm of OFHC copper and lead blocks for shielding. Moreover, 10 cm thickness of OFHC copper was placed on the side of liquid nitrogen dewar which is used for cooling, and preamplifier electronics, in order to supply additional shielding. All these ACV detectors and shielding materials were covered by a plastic bag which function as a purge for the radioactive radon gas.

Table 2.2: Summary of the key information of the four data taking periods with CsI (Tl) scintillation crystal to measure cross-section of $\bar{\nu}_e - e^-$ scattering. The period numbering follows the same scheme as in Ref [62]. (Adopted from [61].)

Period	Data Taking Calendar Time	Reactor ON Live Time (days)	Reactor OFF Live Time (days)	DAQ Live Time (%)	DAQ Threshold (keV)	Average $\bar{\nu}_e$ Flux ($10^{12} cm^{-2} s^{-1}$)	Fiducial Mass (kg)
II	Feb. 2003 - Oct. 2003	95.2	48.4	88.8	100	6.27	43.5
III	Sept. 2004 - Oct. 2005	192	36.6	93.4	500	6.50	40.5
IV	Mar. 2006 - May 2007	204.9	43.5	88.0	500	6.44	51
V	June 2007 - Feb. 2008	132.8	27.6	91.9	500	6.29	57
Combined	Feb. 2003 - Feb. 2008	624.9	156.1	90.4	–	6.39	–

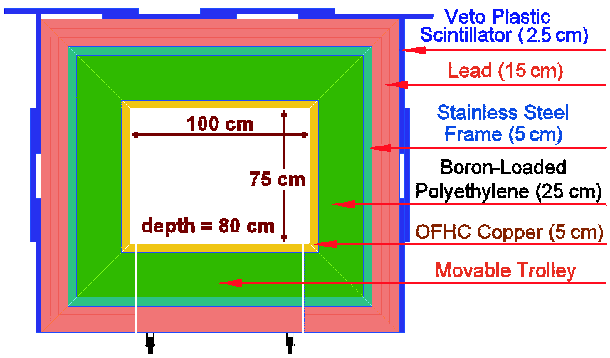

Figure 2.2: The shielding design of KSNL. Similar structures apply to the back and front walls. Detectors and inner shieldings were placed in the inner target volume (Adopted from [61].)

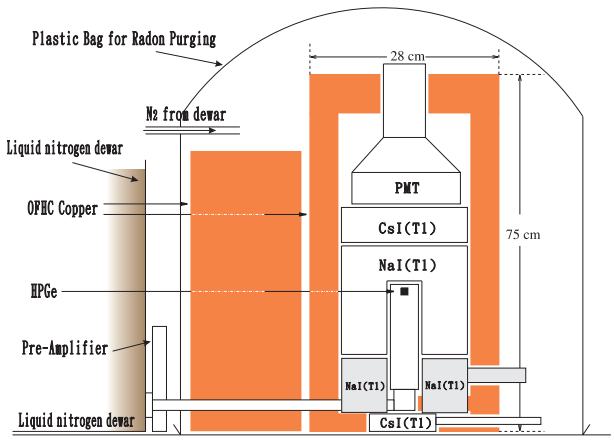

Figure 2.3: Schematic layout of the HPGe with its anti-Compton detectors as well as inner shieldings and radon purge system. (Adopted from [62].)

The electronics and Data acquisition (DAQ) of the HP-Ge detector is shown schematically in Figure 2.4. The signals coming from the preamplifier pass through the spectroscopy amplifiers with different gain factors but with same 4 μs shaping time. Then signal is distributed to triggers where the relevant events to be stored is selected. The signals coming from the ACV, CRV detectors and HP-Ge amplifiers, is recorded by 20 MHz Flash Analog to Digital convertor (FADC) modules after passing the trigger. Also, the timing output of the CRV PMTs is also recorded. A coherent timing and synchronization with the different electronic modules is provided by logic control system. Complete acquisition of delayed signals up to several ms is provided by this system also. With this, it is possible to record cascade events coming from decay series like ^{238}U, ^{235}U, $^{232}T_h$. All the data coming from Logic Control, FADC, and TDC were read out by a VME based DAQ system and connected via PCI-bus to PC running with Linux operating system. The data were saved on hard-disks.

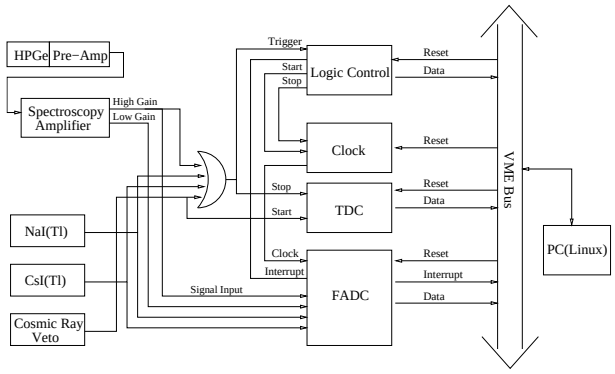

Figure 2.4: Schematic layout of the electronics and data acquisition systems of the HP-Ge and the associated ACV and CRV detectors.(Adopted from [62].)

Scatterings of $\bar{\nu}_e - e^-$ inside the Ge target would manifest as "lone-events" ,uncorrelated with the other detector systems. These events were extracted from raw data through selection criteria, including pulse shape analysis (PSA), anti- Compton vetoes (ACV) and cosmic-ray vetoes (CRV).

Accidental and delayed cascade events were suppressed by PSA. Sometimes, deposit energy due to interaction of two different particles in the detector can be observed in a single event recorded in the the shape of two peaks. This situation can happen due to either an accidental coincidence of two events with a very slight time difference or due to a double hit event like the decay of ^{7}3Ge with 2 gamma particles. This can be seen on Figure 2.5a. Events from the decay of ^{7}3Ge creates a peak in the spectrum at 66 keV. These events can be easily eliminated on the deposit energy versus amplitude plot. They are off the band due to their pulse shape.

For anti-Compton veto (ACV), NaI and CsI (Tl) detectors are used. For anti-Compton tagging, coincidence in in the Ge and NaI or CsI targets are looked for. If there is deposit energy both in Ge and ACV detectors after trigger, that event is eliminated. Amplitude of NaI signal versus event energy is shown on Figure 2.5b. Signal band appears to be at the bottom with zero NaI signal amplitude which means no deposit energy in NaI detector. So only events on that band are kept as clean samples while the others were discarded as anti-Compton events.

Similarly, plastic scintillators which composes the outer part of the shielding are used for cosmic ray veto (CRV). In Figure 2.5c, time difference between the signal from Ge detector and plastic scintillators are shown versus energy. Events on the dark band indicates a time correlation between Ge and plastic scintillator signals. Thus those events appears to be cosmic

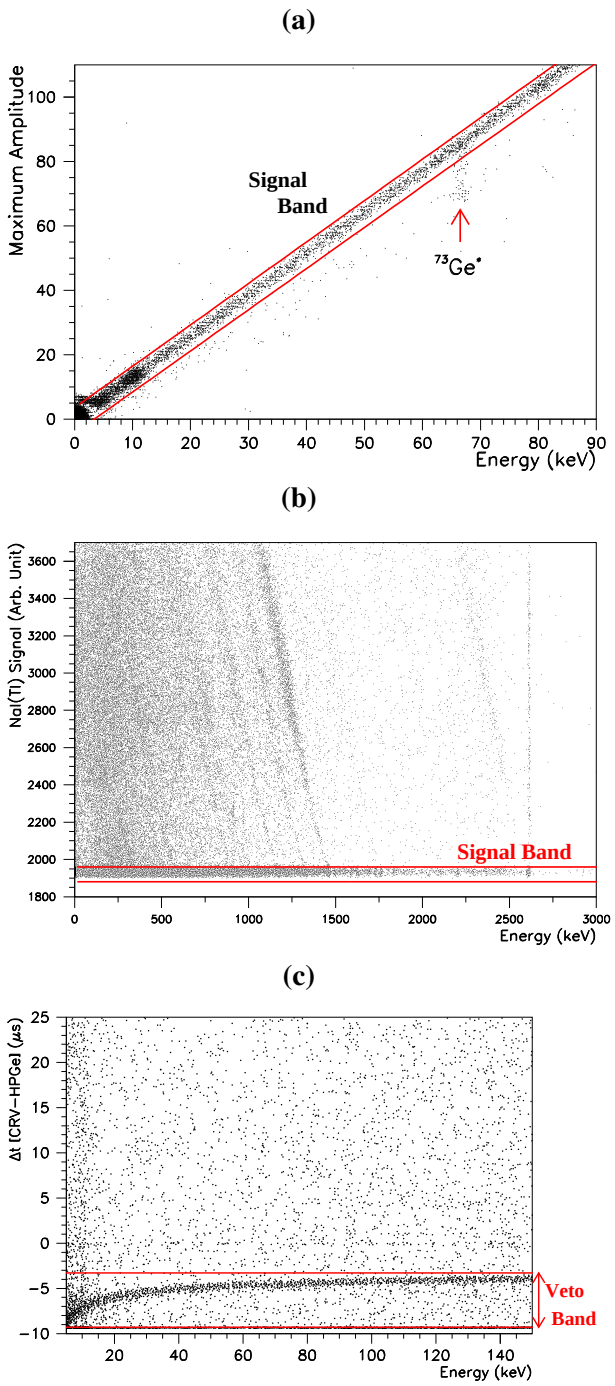

Figure 2.5: Selection procedures of the recorded data : (a) pulse shape analysis, (b) anti-Compton selection, and (c) cosmic-ray veto. (Adopted from [62].)

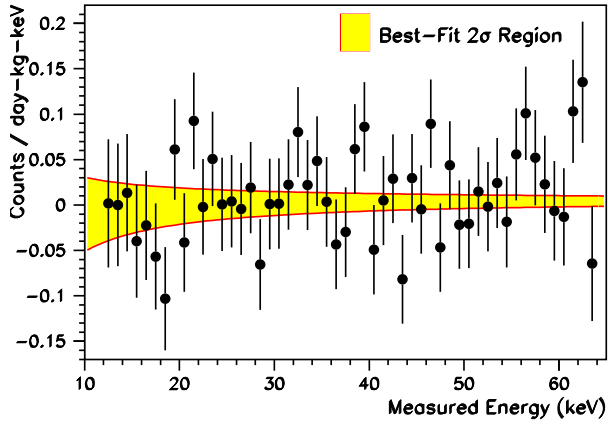

Figure 2.6: The residual plot on the Reactor ON data of all periods combined over the background spectra. (Adopted from [62].)

rays passing through the detector system by hitting both Ge and plastic scintillators.

Recording of each event makes the DAQ system busy for a time interval after the trigger of that event. This time interval is called as the system dead time and during dead time trigger of another event is not possible. Thus live time is the total time during which detector is ready to record the signal and waiting for a new event and it is calculated as the dead time subtracted from total time. Live time is important while calculating the event rates which are normalized for unit time.

For calculation of dead time, random trigger (RT) events are used. These events are artificially created by a clock at a certain rate. However, only a certain percent of these events are recorded due to the system dead time, due to recording of another event. So system live time is calculated from the ratio of recorded RT events to total created RT events.

After applying all cuts and combining the data of all three periods, residual spectrum of the Reactor ON data over the background profile is acquired as shown in Figure 2.6 with the best 2σ region.

2.3 CsI (Tl) Crystal Scintillating Detector

CsI (Tl) scintillating crystal array detector was aimed to use for measurement of electroweak parameters in the energy region of 3-8 MeV. These crystals are packed in a compact array which is used for both target and detector as shown in Figure 2.7. The detector weighed 200

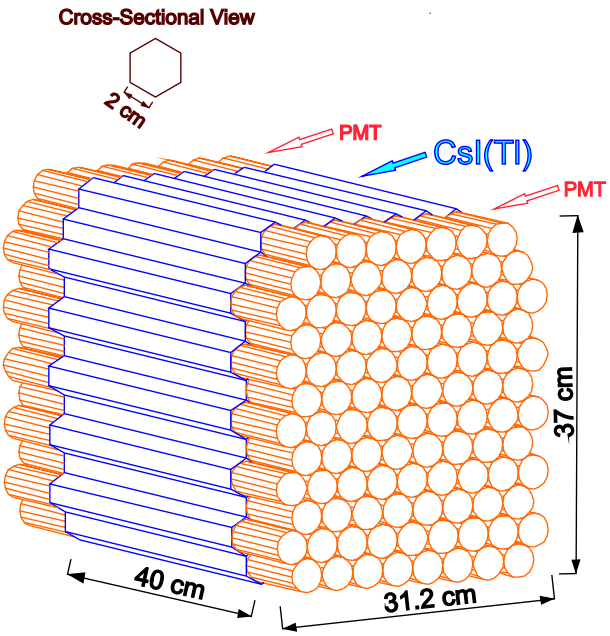

Figure 2.7: Schematic drawing of the CsI (Tl) scintillating crystal array. Light output is recorded by PMTs at both end. (Adopted from [61].)

kg totally. There are two types of crystal modules inside the CsI (Tl) crystal array. One of them is the single crystals with 40 cm length. These type of crystals are placed in the center of the array and used as targets. To increase the shielding the target crystals were put inside a 2.5 mm thick of OFHC copper box. The other type is the 20 cm long crystals. These are glued together optically and placed outer layer of the array so that these crystals can be used for active veto. At both ends of crystals, there are PMTs to read out the light signals. Same DAQ system is used as HP-Ge detectors.

Data analysis is done by using the light output information from both PMTs for each event. Light output recorded by the left and right side of the PMTs are denoted as Q_L and Q_R respectively. Q_L vs Q_R distribution is shown in Figure 2.8. Combination of light outputs from both ends is related to the event energy, but not exactly proportional to the event energy. Because the light output is also effected by the position of the event along the crystal. Hence, an event reconstruction is needed. Certain energy peaks from ambient radiation is expected to appear as some gathered events on diagonal lines. These diagonal lines are used for energy calibration. But they don't exactly constitute exact straight lines but rather bumped lines. So a new parameter Z position, which is the longitudinal position of each event, is defined as:

$$\mathrm{Z} \propto \left[\frac{\beta_i \cdot Q_R - Q_L}{\beta_i \cdot Q_R + Q_L}\right] , \tag{2.1}$$

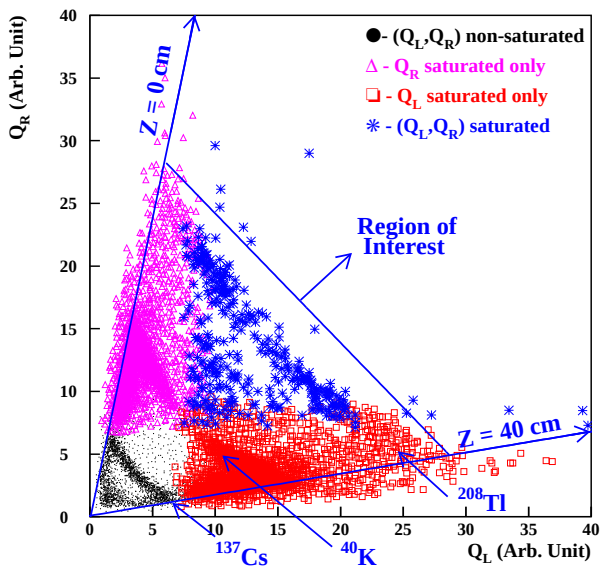

Figure 2.8: Typical Q_L versus Q_R distribution for H1(CRV) events showing the background events of natural sources. Different colors denote whether the PMT signals are saturated at their FADC readout or not. Additional software routines were devised to provide correct energy information for saturated events. (Adopted from [61].)

Parameters β_i's are defined by taking the ^{137}Cs peak as reference by assuming that the ^{137}Cs events must be homogeneously distributed along the crystals.

Using that Z information, event energy is defined as:

$$\mathrm{E} \;=\; a_i \;+\; b_i \cdot e^{-\alpha_i \mathrm{Z}} \cdot \sqrt{Q_L \times Q_R} \;\; . \tag{2.2}$$

where a_i and b_i are calibration parameters obtained by linear fitting to the gamma lines. α_i is the calibration parameter which relates Z to the attenuation of the light outputs along the crystals.

Neutrino-electron scattering cross section is low. As a result, neutrino events are expected to be observed as a single hit in one of the crystals while nothing is observed in the remaining parts of the detector system. Using this fact, events with hits in multiple crystals are eliminated. Also to suppress the cosmic ray and gamma events, correlation with cosmic ray and anti-Compton detectors were sought. In addition, to minimize the gamma background, outermost layers of the detector and the parts of the crystals up to 4 cm of Z position from both sides were rejected.

After a detailed background analysis is done, in which details are given in [61], combined residual spectrum of ON - BKG (Background) spectrum is found as shown in Figure 2.9.

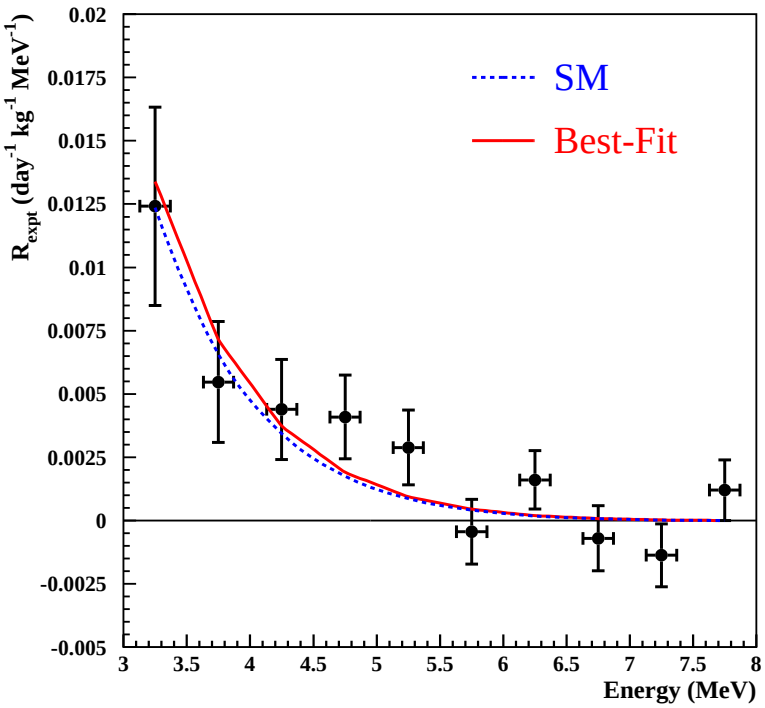

Figure 2.9: The combined residual spectrum $[R_{expt}(\nu) = R_{\mathrm{H1}}(\mathrm{ON}) - R_{\mathrm{H1}}(\mathrm{BKG})]$ in the $3-8$ MeV energy region. The blue and red lines correspond to the SM expectations and to the best-fit of the data, respectively. (Adopted from [61].)

CHAPTER 3

BEYOND THE STANDARD MODEL PHYSICS SEARCH WITH NEUTRINO ELECTRON SCATTERING

3.1 Neutrino Electron Scattering in Standard Model

The elastic scattering of $\bar{\nu}_\mu$ - e^- can take place via neutral current only. As shown in Feynman diagram (Figure 3.1) the weak force is carried by Z^0 boson. Interaction Lagrangian of this interaction is given as;

$$-\mathcal{L} = \frac{\mathcal{G}_{\mathcal{F}}}{\sqrt{2}}\bar{\nu}_\mu\gamma^\mu(1-\gamma^5)\nu_\mu\bar{\mathrm{e}}\gamma_\mu(\mathrm{g_V}-\mathrm{g_A}\gamma^5)\mathrm{e} \tag{3.1}$$

where G_F is the dimensionful Fermi Coupling constant, g_V and g_A are the vector and axial vector couplings respectively. According to SM, $g_V = -\frac{1}{2} + 2\sin^2\theta_\mathrm{W}$ and $g_A = -\frac{1}{2}$, where $\sin^2\theta_\mathrm{W}$ is weak mixing angle (Weinberg angle). With this Lagrangian one can calculate the cross section of the interaction and finds [7, 65];

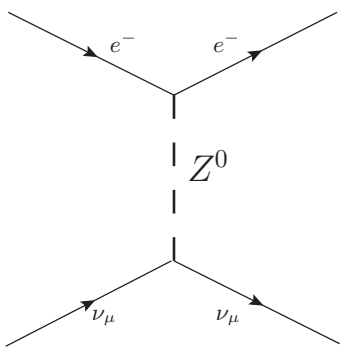

Figure 3.1: $\nu_\mu - e^-$ scattering can only take place via Neutral Current.

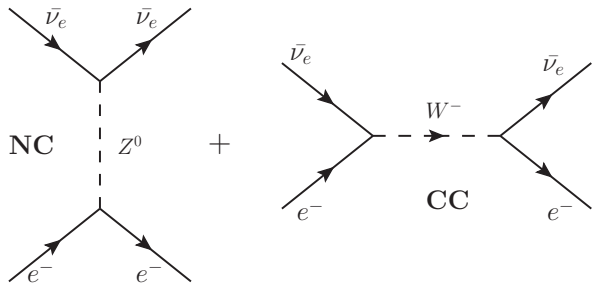

Figure 3.2: Apart from the $\nu_\mu - e^-$ scattering $\bar{\nu}_e - e^-$ scattering can take place both Charged current (CC) and Neutral Current (NC).

$$\begin{aligned}\left[\frac{d\sigma}{dT}(\bar{\nu}_\mu e)\right]_{SM} &= \frac{G_F^2 m_e}{2\pi}\cdot[\ (g_V \pm g_A)^2 \\ &+ (g_V \mp g_A)^2\left(1-\frac{T}{E_\nu}\right)^2 \\ &- (g_V^2 - g_A^2)\ \frac{m_e T}{E_\nu^2}\ ]\ ,\end{aligned} \tag{3.2}$$

where E_ν is the incident neutrino energy, T is the recoiling energy of the electrons. These parameters can be measured by experiments. The upper (lower) sign refers to the interactions with ν_μ ($\bar{\nu}_\mu$).

On the other hand, for $\bar{\nu}_\mathrm{e} - \mathrm{e}^-$ scattering, the interaction can take place via both neutral current (via Z boson exchange) and charged current (via W^- boson exchange) together with the interference between them as shown in Feynman diagram. (Figure 3.2) The cross-section can be obtained by making the replacement $g_{V,A} \rightarrow (g_{V,A} + 1)$. Therefore the cross section for $\bar{\nu}_\mathrm{e} - \mathrm{e}^-$ scattering, which is the case for reactor neutrino experiments is found as; [7, 65]

$$\begin{aligned}\left[\frac{d\sigma}{dT}(\bar{\nu}_e e)\right]_{SM} &= \frac{G_F^2 m_e}{2\pi}\cdot[\ (g_V - g_A)^2 \\ &+ (g_V + g_A + 2)^2\left(1-\frac{T}{E_\nu}\right)^2 \\ &- (g_V - g_A)(g_V + g_A + 2)\frac{m_e T}{E_\nu^2}\ ].\end{aligned} \tag{3.3}$$

By defining chiral couplings g_L and g_R as;

$$\begin{aligned} g_L &= \frac{1}{2}(g_V + g_A) = -\frac{1}{2} + \sin^2\theta_\mathrm{W} \quad \text{and} \\ g_R &= \frac{1}{2}(g_V - g_A) = \sin^2\theta_\mathrm{W}\ \ , \end{aligned} \tag{3.4}$$

then equation 3.3 becomes in terms of chiral couplings as;

$$\left[\frac{d\sigma}{dT}(\bar{\nu}_e e)\right]_{SM} = \frac{2G_F^2 m_e}{\pi} \cdot [g_R^2 + (g_L+1)^2(1-\frac{T}{E_\nu})^2 - g_R(g_L+1)\frac{m_e T}{E_\nu^2}] \quad . \tag{3.5}$$

If we interchange g_L and g_R ($g_L \leftrightarrow g_R$) in equation 3.5, then we get the cross section for the $\bar{\nu}_e - e^-$ scattering.

3.2 Non Standard Interactions of Neutrinos

Different from the neutrino oscillation phenomena, flavor changing interactions between neutrinos and matter could be an alternative solution to solar and atmospheric neutrino anomaly. As shown in Figure 3.3, the reason of detecting much more muon type neutrinos than the predicted may be that, either electron neutrinos, which are emerged in the source due to muon decay, oscillated to muon type neutrinos during the way or lepton number is violated and $\mu^+ \rightarrow e^+ + \nu_\mu + \bar{\nu}_\mu$ interaction take place and emerging neutrinos are already muon type. Another situation could take place in detector side. There may be two reasons that we observe μ^- in the detector. First, ν_e oscillated into ν_μ and muon neutrinos interacted with neutrons to produce proton and muon. Second, lepton number is violated and $\nu_e + n \rightarrow p + \mu^-$ take place and we observe muons in the detector. If this is the case, then neutrinos should have been interacting differently with matter than Standard Model prediction. Even if neutrino oscillation, which implies neutrino mixing and neutrinos being massive, exists there is still contradictions with SM since neutrinos are massless in SM. Therefore trying to explain the atmospheric and solar neutrino anomaly is one of the reason why we need theories beyond SM. These new interactions apart from SM prediction is generally called as Non-Standard Interactions (NSI).

NSI can cause lepton number violation therefore it has been thought as an alternative solution to neutrino oscillation phenomena [66]. Although KamLAND [67] experimentally confirmed the large mixing angle oscillation explanation [7] and rejected the NSI of neutrinos as an explanation to neutrino anomalies, NSI still can be important in the sense that it can affect the neutrino oscillation parameters.

NSI was not only a candidate to explain solar and atmospheric neutrino anomalies but also emerges in beyond the SM theories [68] where neutrino gain mass like, seesaw type models,

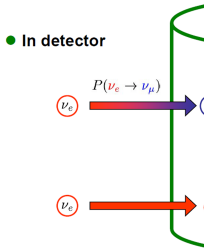

Figure 3.3: Both lepton number violation and neutrino oscillation phenomena could be an explanation of atmospheric and solar neutrino anomaly. The possibilities that occur in source (above) and detector (below) is shown.

low energy Supersymmetry [SUSY] with breaking of R-parity, models acquiring mass radiatively due to the presence of extra Higgs boson, in unified SUSY models as a renormalization effect etc.

NSI phenomenology is studied in a wide range of areas like; reactor neutrinos [69], solar neutrinos [66, 70, 71, 72, 73, 74], atmospheric neutrinos [75, 76, 77, 78, 79, 80], supernova neutrinos [81, 82], neutrino electron scattering [83, 84], neutrino nucleus scattering [84, 85], e$^-$ e^+ colliders [86] etc. Although there are studies depending on concrete models [87, 88, 89, 90, 91, 92, 93, 94], most studies use model independent approach [87, 95, 96, 97, 98].

In general, NSI of neutrinos can be described in a model independent way, just modifying the SM electroweak interactions in the usual $V - A$ (vector-axial) form with new couplings as illustrated schematically in Figure 3.4.

A model independent way of introducing NSI in the $\bar{\nu}_\alpha - e^-$ scattering is described by an effective Lagrangian:

$$\mathscr{L}_{\text{eff}} = -\epsilon^{eP}_{\alpha\beta} 2\sqrt{2} G_F (\bar{\nu}_\alpha \gamma_\rho L \nu_\beta)(\bar{e}\gamma^\rho P e) \tag{3.6}$$

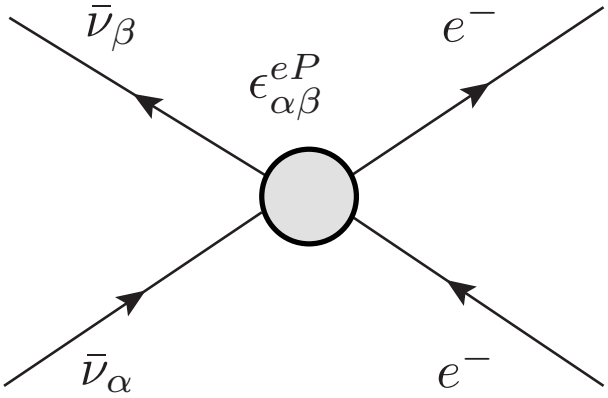

Figure 3.4: NSI of neutrinos can be written as a model independent way like four fermi interaction with new couplings.

where $\epsilon^{eP}_{\alpha\beta}$ is a constant and describes the strength of the NSI with respect to G_F, P corresponds to chiral operators of L or R which are $(1 \pm \gamma^5)/2$, respectively, and $(\alpha\ \beta)$ stands for lepton flavor e, μ or τ. The cases where $\alpha = \beta$ and $\alpha \neq \beta$ corresponds to Non-Universal (NU) NSI, which means flavor type is conserved in the interaction, and Flavour-Changing (FC) NSI, which means neutrino type is changed after interaction, respectively. For reactor experiments α corresponds to e^-, since radioactive source produces $\bar{\nu}_e$ via β decay.

By adding the SM Lagrangian to the effective Lagrangian of NSI, the cross-section formula for $\bar{\nu}_e - e^-$ scattering, $\bar{\nu}_\mathrm{e} + e \rightarrow \bar{\nu}_\mathrm{e} + e$, takes the form as given by [99, 100]

$$\begin{aligned}\left[\frac{d\sigma}{dT}\right]_{SM+NSI} = & \frac{2G_F^2 m_e}{\pi} \cdot [\left(\tilde{g}_R^2 + \sum_{\alpha\neq e} |\epsilon^{eR}_{\alpha e}|^2\right) \\ & + \left((\tilde{g}_L + 1)^2 + \sum_{\alpha\neq e} |\epsilon^{eL}_{\alpha e}|^2\right)\left(1 - \frac{T}{E_\nu}\right)^2 \\ & - \left(\tilde{g}_R(\tilde{g}_L + 1) + \sum_{\alpha\neq e} |\epsilon^{eR}_{\alpha e}||\epsilon^{eL}_{\alpha e}|\right)\frac{m_e T}{E_\nu^2}] \quad ,\end{aligned} \tag{3.7}$$

where $\tilde{g}_L = g_L + \varepsilon^{\mathrm{eL}}_{\mathrm{ee}}$ and $\tilde{g}_R = g_R + \varepsilon^{\mathrm{eR}}_{\mathrm{ee}}$. To get the cross section formula for $\nu_e - e^-$ scattering, one needs to change L with R, $L \leftrightarrow R$ and vice versa. We have six NSI parameters, two of them, $\epsilon^{eL,R}_{ee}$, correspond to NU NSI parameter, four of them, $\epsilon^{eL,R}_{e\mu}$ and $\epsilon^{eL,R}_{e\tau}$, correspond to FC NSI. Reactor experiments are more sensitive to NSI parameters, since the oscillation effects do not play an important role in the interaction since baseline is too short for the oscillations.

3.3 Unparticle Physics

In Standard Model, the particles obey the relation $p^\mu p_\mu = m^2$ that is $E^2 - p^2 = m^2$. Looking at the universal constants as "c" and "$\hbar$", we can see that if time and space are scaled up then energy and momentum must be scaled down and vice versa. So since the particle we know have definite masses, Standard Model does not have the property of scale invariance. Roughly, scale invariance means that the physical laws or properties of the objects do not change even if the length scale (energy) changes. Hence, massless particles have the scale invariance property. For instance, if a massless particle (photon can be an example for it) is in a state (E_i, p_i) then even if you make a scaled state with $(\lambda E_i, \lambda p_i)$ where λ is a scalar rescaling parameter nothing changes in physical laws.

The "things" described by scale invariant theories can not have definite mass unless that mass is zero. Therefore, these "things" having different properties from the particles we know are called as "unparticle."

A scale invariant sector may exist in very high energies. This sector can be described by Banks-Zaks (BZ) fields which is related with gauge theories with non integer number of fermions [9]. BZ fields has its own gauge group and do not couple to the SM fields. Since it is very well known that particles, described by SM fields have definite mass, if the scale invariant sector exists, it must have been decoupled at an energy scale. To be inspired by Banks-Zaks fields, Georgi [10] proposed an idea that both SM fields and BZ fields may coexist in a high energy scale and although BZ fields do not couple to the SM fields, there may exist a field with mass scale $M_{\mathcal{U}}$, carrying both gauge interactions of SM and BZ fields [10, 60]. The strength of this interaction is much less due to the high mass scale $M_{\mathcal{U}}$. The interaction between these two sectors below the mass scale $M_{\mathcal{U}}$ can be described by

$$\frac{1}{M_{\mathcal{U}}^k} O_{BZ} O_{SM} (k > 0) \tag{3.8}$$

where O_{BZ} and O_{SM} corresponds to BZ and SM field operators with mass dimensions d_{BZ} and d_{SM} respectively and $k = d_{SM} + d_{BZ} - 4$.

As Georgi pointed out, below an energy scale, $\Lambda_{\mathcal{U}}$, BZ operators turn into unparticle operators with a non-integer scaling dimension d and the equation above takes the form;

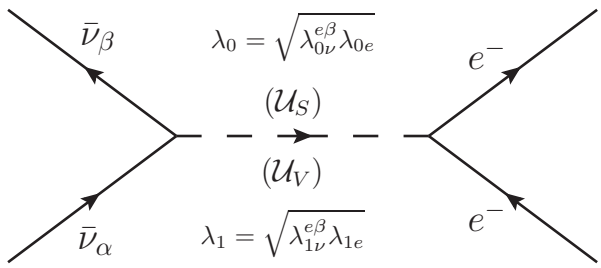

Figure 3.5: Interactions of neutrino with electron via exchange of virtual scalar $\mathcal{U}_S$ and vector $\mathcal{U}_V$ unparticle.

$$\frac{C_{\mathcal{U}}\Lambda_{\mathcal{U}}{}^{d_{BZ}-d}}{M_{\mathcal{U}}^{k}} O_{\mathcal{U}} O_{SM} \tag{3.9}$$

where $C_{\mathcal{U}}$ is a dimensionless coupling constant.

Unparticle effects can be studied in accelerator experiments [101] through their direct production, the signatures of which are missing energy in the detectors. An alternative method is to probe the virtual effects of unparticles which act as mediators in the interactions [10, 101]. For reactor neutrino experiments the way to search unparticle effects is looking for the virtual effects which will be discussed in detail in Chapter 6.

3.3.1 Neutrino-Electron Scattering via Unparticle Exchange

The interaction Lagrangians for $\nu_\alpha + e \rightarrow \nu_\beta + e$ via virtual scalar and vector unparticle exchange as depicted in Figure 3.5 are given, respectively, by [101, 102, 103, 104]

$$\mathscr{L}_{\mathrm{J}=0} = \frac{\lambda_{0e}}{\Lambda_{\mathcal{U}}^{d_S-1}}\,\bar{e}e\,O_{\mathcal{U}} + \frac{\lambda_{0\nu}^{\alpha\beta}}{\Lambda_{\mathcal{U}}^{d_S-1}}\,\bar{\nu}_\alpha\nu_\beta\,O_{\mathcal{U}} \quad \text{and} \tag{3.10}$$

$$\mathscr{L}_{\mathrm{J}=1} = \frac{\lambda_{1e}}{\Lambda_{\mathcal{U}}^{d_V-1}}\,\bar{e}\gamma_\mu e\,O_{\mathcal{U}}^{\mu} + \frac{\lambda_{1\nu}^{\alpha\beta}}{\Lambda_{\mathcal{U}}^{d_V-1}}\,\bar{\nu}_\alpha\gamma_\mu\nu_\beta\,O_{\mathcal{U}}^{\mu}\,, \tag{3.11}$$

where λ_{Je} and $\lambda_{J\nu}^{\alpha\beta}$ are the corresponding coupling constants with $J = 0, 1$ denoting scalar and vector unparticle interactions, respectively.

The cross-section of $\bar{\nu}_e$−e scattering with scalar unparticle exchange is given by

$$\left(\frac{d\sigma}{dT}\right)_{\mathcal{U}_S} = \frac{f_0^2(d_S)}{\Lambda_{\mathcal{U}}^{4d_S-4}}\,\frac{2^{2d_S-6}}{\pi E_\nu^2}\,(m_e T)^{2d-3}\,(T + 2m_e)\ , \tag{3.12}$$

where

$$f_0(d_S) = \frac{\lambda_{0\nu}^{\alpha\beta}\lambda_{0e}}{2\sin(d_S\pi)} A_0(d_S) \tag{3.13}$$

and the normalization constant $A_0(d_{\mathcal{S}})$ is given by:

$$A_0(d_{\mathcal{S}}) = \frac{16\pi^{5/2}}{(2\pi)^{2d_{\mathcal{S}}}} \frac{\Gamma(d_{\mathcal{S}} + 1/2)}{\Gamma(d_{\mathcal{S}} - 1)\Gamma(2d_{\mathcal{S}})} \quad . \tag{3.14}$$

The interference effects with SM are negligible due to suppression by factors of $m_\nu/\Lambda_{\mathcal{U}}$. Therefore, it is not necessary to differentiate flavor conserving (FC) and violating (FV) scalar UP interactions.

The cross-section of $\bar{\nu}_{\mathrm{e}} - \mathrm{e}^-$ scattering via vector UP exchange is

$$\begin{aligned} \left(\frac{d\sigma}{dT}\right)_{\mathcal{U}_{\mathcal{V}}} &= \frac{1}{\pi} \frac{f_1^2(d_{\mathcal{V}})}{\Lambda_{\mathcal{U}}^{4d_{\mathcal{V}}-4}} 2^{2d_{\mathcal{V}}-5} m_e^{2d_{\mathcal{V}}-3} T^{2d_{\mathcal{V}}-4} \\ &\times \left[1 + \left(1 - \frac{T}{E_\nu}\right)^2 - \frac{m_e T}{E_\nu^2}\right] \quad , \end{aligned} \tag{3.15}$$

where $f_1(d_{\mathcal{V}})$ follows a similar expression as Eq. 3.13, making the replacement $\lambda_{0\nu}^{\alpha\beta}\lambda_{0e} \rightarrow \lambda_{1\nu}^{\alpha\beta}\lambda_{1e}$ and $A_0(d_{\mathcal{S}}) \rightarrow A_1(d_{\mathcal{V}})$. Unlike the scalar UP case, the interference effects with SM also contribute in the vector UP interactions:

$$\begin{aligned} \left(\frac{d\sigma}{dT}\right)_{\mathcal{U}_{\mathcal{V}}-\mathcal{SM}} &= \frac{\sqrt{2}G_F}{\pi} \frac{f_1(d_{\mathcal{V}})}{\Lambda_{\mathcal{U}}^{2d_{\mathcal{V}}-2}} (2m_e T)^{d_{\mathcal{V}}-2} m_e \\ &\times [g_R + (g_L + 1)\left(1 - \frac{T}{E_\nu}\right)^2 \\ &- \frac{(g_L + g_R + 1)}{2} \frac{m_e T}{E_\nu^2}] \, . \end{aligned} \tag{3.16}$$

The FV and FC cross-sections for vector UP are therefore given by Eq. 3.15 and the sum of Eq. 3.15 and Eq. 3.16, respectively.

CHAPTER 4

ANALYSIS AND RESULTS[1]

If there is a new type of interaction apart from Standard Model, we expect that this new kind of interaction will contribute to the number of events that we measure in $\bar{\nu}_e - e^-$ scattering experiment. We assume that Standard Model predictions is what we expect to measure in experiments. The event rate (R), expressed in units of $kg^{-1}day^{-1}$, including the new physics (NP) effect to the SM interaction, can be written as;

$$R_{\mathcal{NP}+\mathcal{SM}} \;=\; t\,\rho_e \int_T \int_{E_\nu} \left(\frac{d\sigma}{dT}\right)_{\mathcal{NP}+\mathcal{SM}} \frac{d\phi_{(\bar{\nu}_e)}}{dE_\nu}\, dE_\nu\, dT \;\;, \tag{4.1}$$

where ρ_e is the electron number density per kg of target mass, t is the data taking period (which is one day for our case), T is the recoiling energy of electrons and $d\phi_{\bar{\nu}_e}/dE_\nu$ denotes the neutrino spectrum. NP corresponds to any new physics effect to Standard Model, for our case which is Non-Standard Interactions and Unparticles. The relation between the maximum recoil energy of electron (T) and incoming neutrino energy (E_ν) is found as;

$$T_{max} = \frac{2E_\nu}{m_e + 2E_\nu}$$

As it is seen from this equation, if the mass of the target increases, T_{max} decreases and it becomes a challenge for experiments to detect. This is the most important reason why neutrino nucleus coherent scattering has not been observed yet. However, there are continuing studies trying to observe neutrino nucleus coherent scattering [64].

For the analysis of NSI and Unparticles, three different data sets are used in which details are given in Chapter 2. In summary, these data sets each of which have different energy range are [60];

[1] This work is published in [60]. All the figures and even some of the text is directly adopted from that paper.

DS1-CsI(Tl): Data with 29882/7369 kg-days of Reactor ON/OFF exposure of a CsI(Tl) crystal scintillator array [61] with a total mass of 187 kg. Analysis range is 3 − 8 MeV. From the excess of events in the ON−OFF residual spectrum, the SM electroweak angle was measured to be $\sin^2\theta_W = 0.251 \pm 0.031(stat) \pm 0.024(sys)$ which improved over previous results from $\bar{\nu}_e$−e scattering and was comparable to those from ν_e−e experiments.

DS2-HPGe: Data with 570.7/127.8 kg-days of Reactor ON/OFF exposure taken with a high-purity germanium (HPGe) detector [62] with a target mass of 1.06 kg. Analysis threshold of 10 keV with a background level of ~ 1 kg^{-1}keV^{-1}day^{-1} was achieved. The low threshold allowed sensitive limits on neutrino magnetic moments to be derived from the ON−OFF residual spectrum.

DS3-ULEGe: Data with 0.338 kg-days of Reactor ON exposure taken with an ultra-low-energy germanium (ULEGe) detector array [6] with a total mass of 20 g and a threshold of 220±10 eV. The sub-keV threshold opened a window of studying WIMP dark matter with mass less than 10 GeV.

The event rate (R_{expt}) of three data sets (DS1−3) are displayed in Figure 4.1a,b&c, respectively. The SM contributions from $\bar{\nu}_e$−e are superimposed in (a) and (b), and are out of range at $\sim 10^{-3}$ kg^{-1}keV^{-1}day^{-1} in (c). Every Data Set has its own energy ranges and these are depicted in Figure 4.2 and Figure 4.5. For data sets (DS1−2) we have the information of reactor ON and OFF periods separately. Data taken in OFF periods provide model-independent means of background subtraction. Therefore, for these two sets of data for searching Unparticle and NSI effects a minimum χ^2 fit method can be performed like;

$$\chi^2 = \sum_{i=1} \left[\frac{R_{expt}(i) - [R_{SM}(i) + R_{NP}(i)]}{\Delta_{stat}(i)} \right]^2 , \tag{4.2}$$

where $R_{SM}(i)$ and $R_{NP}(i)$ are the expected event rates on the ith data bin due to the SM and NP(=NSI or UP) contributions, respectively, while $\Delta_{stat}(i)$ is the corresponding uncertainty of the measurement. On the contrary to these two data sets, for DS3-ULEGe, there was no corresponding Reactor OFF data so that the conventional Reactor ON-OFF background subtraction and a χ^2 min analysis were not possible. Therefore as in the case for WIMP analysis [6, 105] ”Binned Poisson” method which is so common for Dark Matter search is

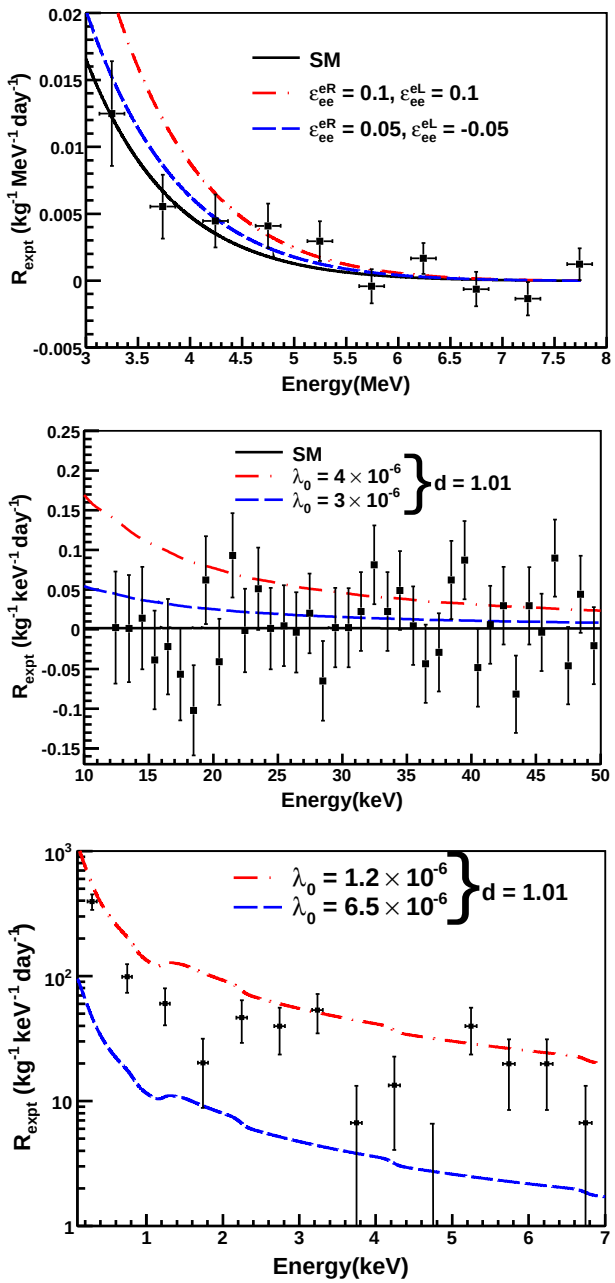

Figure 4.1: The three data sets adopted for this analysis. Observable NSI or UP spectra at allowed and excluded parameter space are superimposed. Top: (a) DS1-CsI(Tl) Reactor ON−OFF [62], showing SM+NSI with NSI at $(\varepsilon_{ee}^{eR}, \varepsilon_{ee}^{eL})$ = (0.1,0.1) and (0.05,−0.05). Middle: (b) DS2-HPGe Reactor ON−OFF [61], showing SM+UP with $\lambda_0 = 4 \times 10^{-6}$ versus 3×10^{-6} at $d_S = 1.01$. Bottom: (c) DS3-ULEGe Reactor ON only [6], showing SM+UP with $\lambda_0 = 1.2 \times 10^{-5}$ versus 6.5×10^{-6} at $d_S = 1.01$. The SM contributions from $\bar{\nu}_e$−e are displayed in (a) and (b) as comparison, and are out of range at $\sim 10^{-3}$ kg^{-1}keV^{-1}day^{-1} in (c).

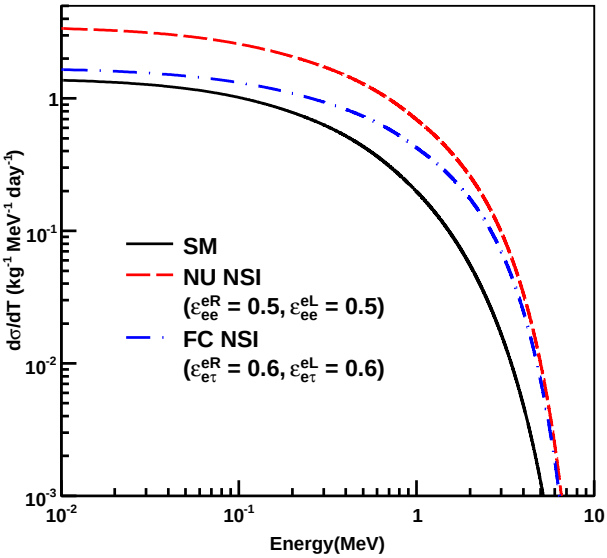

Figure 4.2: Differential cross-section as function of the recoil energy T with typical reactor-$\bar{\nu}_e$ spectra. NSI at coupling parameters relevant to this work using CsI(Tl) as target is shown.

used [106]. Background assumption was not made but instead upper bounds are put for NSI and unparticle parameters since they could not be larger than the observed signals.

4.0.2 Non-Standard Neutrino Interactions

The NSI parameters are constrained by the accuracy of the SM cross-section measurements. The contribution of Non-Standard Interaction to the observed number of events, can be calculated by Eq. 4.1 using the cross section formula given in Eq. 3.7. For the NSI analysis DS1-CsI(Tl) data set is used. And the sensitivity of this experiment data to NSI parameters are shown in Figure 4.2.

We present our results in two different ways. First we will perform one parameter at a time analysis. We will vary only one parameter each time and fix the other parameters to zero. From $\bar{\nu}_e - e^-$ scattering experiments, we can only put bounds on the parameters of $\varepsilon_{ee}^{eL,R}$ for NU NSI and $\varepsilon_{e\tau}^{eL,R}$, $\varepsilon_{e\mu}^{eL,R}$ for the FC NSI. These parameters are the fitting variables in the minimum χ^2 analysis. Applying one parameter at a time analysis technique, new limits on $\varepsilon_{ee}^{eL,R}$, $\varepsilon_{e\mu}^{eL,R}$ and $\varepsilon_{e\tau}^{eL,R}$ were derived. It is important to note that the results on $\varepsilon_{e\mu}^{eL,R}$ and $\varepsilon_{e\tau}^{eL,R}$ are identical since their roles are symmetrical such that one-dimensional analysis cannot differentiate their effects. Our results are given in Table 4.1. For the flavor changing parameters $\varepsilon_{e\tau}^{eL,R}$ and $\varepsilon_{e\mu}^{eL,R}$ we applied a fit for the squares of them since the cross section vary as $[\varepsilon_{e\mu}^{eL,R}]^2([\varepsilon_{e\tau}^{eL,R}]^2)$,

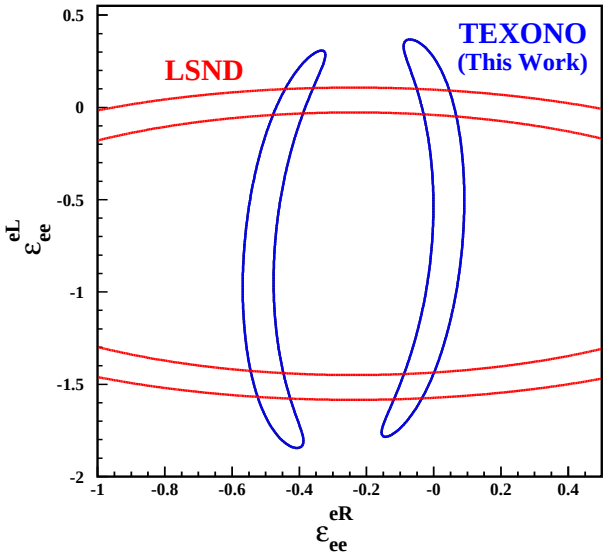

Figure 4.3: The allowed region at 90% CL for NU NSI parameters of ε_{ee}^{eL} and ε_{ee}^{eR}; The allowed regions from the LSND experiment on ν_e−e are superimposed.

respectively. To be able to set upper bounds at 90% C.L for the $\varepsilon_{e\tau}^{eL,R}$ and $\varepsilon_{e\mu}^{eL,R}$ the statistical method given in [107] is used as in the case for searching magnetic moment of neutrinos [62].

Moreover, for comparison we also list the constraints from LSND which is ν_e−e measurement [99] experiment and those from a combined analysis with data from LEP, CHARM, LSND, and previous reactor experiments [100], as well as a model-independent analysis on $\varepsilon_{e\mu}^{eL,R}$. Second, since there are strong bounds on lepton flavor violating processes we will assume that FC NSI parameters do not contribute and only take into account NU NSI parameters in which for $\bar{\nu}_e - e^-$ scattering experiments those are; ε_{ee}^{eL}, ε_{ee}^{eR}. Taking into account the effect of both ε_{ee}^{eL}, ε_{ee}^{eR} parameters and applying χ^2 test we get the sensitivity plot in 90%C.L as shown in Figures 4.3. Since the present bounds are set by LSND [99], which is a ν_e e scattering experiment, we decided to plot both results in the same graph to compare the results so that we can find better sensitivity on the parameters using the ν_e and $\bar{\nu}_e$ scattering topology which makes our ellipse shaped sensitivity plot orthogonal to the LSND one [99]. Moreover, from a two parameter analysis, we assumed that only one type of flavor changing is favored, and displayed the allowed region for the parameters $\varepsilon_{e\tau}^{eL}$ and $\varepsilon_{e\tau}^{eR}$ at 90%C.L as shown in Figure 4.4. Due to the same reason as mentioned above, LSND [99] result is overlaid. As seen from 4.2 the cross section form becomes equal for the parameters $(\varepsilon_{e\mu}^{eL}, \varepsilon_{e\mu}^{eR})$ and $(\varepsilon_{e\tau}^{eL}, \varepsilon_{e\tau}^{eR})$ when two parameter analysis is applied. Therefore our result is same for $(\varepsilon_{e\mu}^{eL}, \varepsilon_{e\mu}^{eR})$ and $(\varepsilon_{e\tau}^{eL}, \varepsilon_{e\tau}^{eR})$.

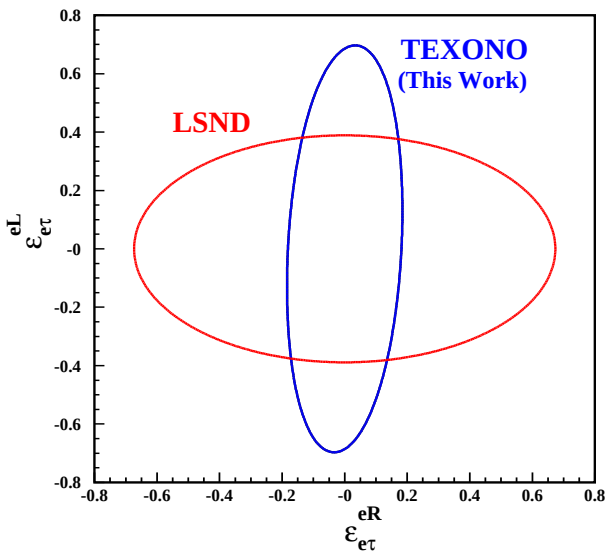

Figure 4.4: FC NSI parameters of $\varepsilon_{e\tau}^{eL}$ and $\varepsilon_{e\tau}^{eR}$ from DS1-CsI(Tl) on $\bar{\nu}_e$−e. The allowed regions from the LSND experiment on ν_e−e are superimposed.

4.0.3 Unparticle Physics Parameters

Unparticle effects can be seen by direct production of unparticles, in which the signature will be the missing energy in the detector or by virtual effects of unparticles which means unparticles act as a mediator particle in the interaction [10, 11]. The first method is the case in accelerators [101]. A single photon production ($e^- + e^+ \rightarrow \gamma + X$) in LEP can be an example of searching via direct detection. X can be any beyond the SM particle even ($\bar{\nu}\nu$), and in this case unparticle for instance. The way to detect is to look for the missing energy in the detectors and in this case ($\bar{\nu}\nu$) interaction will be its background [104]. For the reactor neutrinos we can only probe the virtual effects of unparticles. As in the NSI analysis we will search for the excess number of events in the detector apart from SM prediction.

As it can be seen from the cross section formulas of $\bar{\nu}_e - e^-$ scattering by scalar and vector unparticle exchange given in the Eq. 3.12 and Eq. 3.15, three sets of parameters characterize the unparticle interactions and can be probed experimentally: (i) unparticle energy scale $\Lambda_{\mathcal{U}}$, (ii) unparticle mass dimensions $d_{\mathcal{S}}$ and $d_{\mathcal{V}}$, as well as (iii) coupling constants $\lambda_0 \equiv \sqrt{\lambda_{0\nu}^{e\beta}\lambda_{0e}}$ and $\lambda_1 \equiv \sqrt{\lambda_{1\nu}^{e\beta}\lambda_{1e}}$ for the scalar and vector UP interactions, respectively. To conserve the unitarity and require the physical observable meaningful, scalar dimension d should lie in the range of $1 < d_{\mathcal{S}} < 2$ [109]. However, for the vector unparticle case the range of dimension parameter is not as narrow as in the scalar unparticle case and unitarity imposes only lower

Table 4.1: Constraints at 90% CL due to one-parameter fits on the NSI couplings. The results are presented as "best-fit ± statistical error ± systematic error". Bounds from LSND [99] and combined data [100], as well as from a model-independent analysis [108] are compared with those of this work. The projected statistical sensitivities correspond to a potential measurement of the SM cross-section at 2% accuracy [61].

		TEXONO (This Work)				LSND [99]	Combined [100]	Ref. [108]
	NSI Parameters	Measurement Best-Fit	χ^2/dof	Bounds at 90% CL	Projected Sensitivities	Bounds at 90% CL		
NU {	ε_{ee}^{eL}	ε_{ee}^{eL} = 0.03 ± 0.26 ± 0.17	8.9/9	$-1.53 < \varepsilon_{ee}^{eL} < 0.38$	±0.015	$-0.07 < \varepsilon_{ee}^{eL} < 0.11$	$-0.03 < \varepsilon_{ee}^{eL} < 0.08$	$\lvert\varepsilon_{ee}^{eL}\rvert < 0.06$
	ε_{ee}^{eR}	ε_{ee}^{eR} = 0.02 ± 0.04 ± 0.02	8.7/9	$-0.07 < \varepsilon_{ee}^{eR} < 0.08$	±0.002	$-1.0 < \varepsilon_{ee}^{eR} < 0.5$	$0.004 < \varepsilon_{ee}^{eR} < 0.151$	$\lvert\varepsilon_{ee}^{eR}\rvert < 0.14$
FC {	$\varepsilon_{e\mu}^{eL}$	$\varepsilon_{e\mu}^{eL^2}(\varepsilon_{e\tau}^{eL^2})$ = 0.05 ± 0.27 ± 0.24	} 8.9/9	$\lvert\varepsilon_{e\mu}^{eL}\rvert < 0.84$	±0.052	–	$\lvert\varepsilon_{e\mu}^{eL}\rvert < 0.13$	$\lvert\varepsilon_{e\mu}^{eL}\rvert < 0.1$
	$\varepsilon_{e\tau}^{eL}$			$\lvert\varepsilon_{e\tau}^{eL}\rvert < 0.84$	±0.052	$\lvert\varepsilon_{e\tau}^{eL}\rvert < 0.4$	$\lvert\varepsilon_{e\tau}^{eL}\rvert < 0.33$	$\lvert\varepsilon_{e\tau}^{eL}\rvert < 0.4$
	$\varepsilon_{e\mu}^{eR}$	$\varepsilon_{e\mu}^{eR^2}(\varepsilon_{e\tau}^{eR^2})$ = 0.008 ± 0.015 ± 0.012	} 8.7/9	$\lvert\varepsilon_{e\mu}^{eR}\rvert < 0.19$	±0.007	–	$\lvert\varepsilon_{e\mu}^{eR}\rvert < 0.13$	$\lvert\varepsilon_{e\mu}^{eR}\rvert < 0.1$
	$\varepsilon_{e\tau}^{eR}$			$\lvert\varepsilon_{e\tau}^{eR}\rvert < 0.19$	±0.007	$\lvert\varepsilon_{e\tau}^{eR}\rvert < 0.7$	$0.05 < \lvert\varepsilon_{e\tau}^{eR}\rvert < 0.28$	$\lvert\varepsilon_{e\tau}^{eR}\rvert < 0.27$

bounds of d as $d_{\mathcal{V}} \geq 3$ [110]. Unparticle energy scale, $\Lambda_{\mathcal{U}}$ is taken as 1 TeV in most of the searches [103, 104, 111]. As d gets larger the effect of unparticle becomes too small to be observed. Since there is no upper bounds on $d_{\mathcal{V}}$ for vector unparticle case we will represent our analysis for $3 < d_{\mathcal{V}} < 4$ to get the idea about the behavior of the coupling constant parameters.

The differential cross-sections of the UP interactions using Ge as target are displayed in Figure 4.5 with the SM contributions superimposed for comparison. The saw-tooth structures for $T \lesssim 1$ keV are due to suppression by the atomic binding energy [112].

From the cross section formula given in Eq. 3.12 and from the Figure 4.5, it can be seen that for the small recoil energies, cross section becomes larger in the range of $d < 3/2$. Due to this reason low energy threshold experiments provides better sensitivity for smaller d values. Since depending on the mass dimension parameter $d_{\mathcal{S}}$, the sensitivity of Unparticle effects vary according to energy range of the experiment, all three data sets were used in the Unparticle analysis for their complementarity. The phenomenological study of unparticle using the threshold value of DS2-HPGe detector was also done in [103]. However, the real data with corrected cross section formula [104] is analyzed in this study and the results are compared with the previous studies.

Similar to the NSI analysis, we add the cross section of $\bar{\nu}_e - e^-$ scattering with scalar unpar-

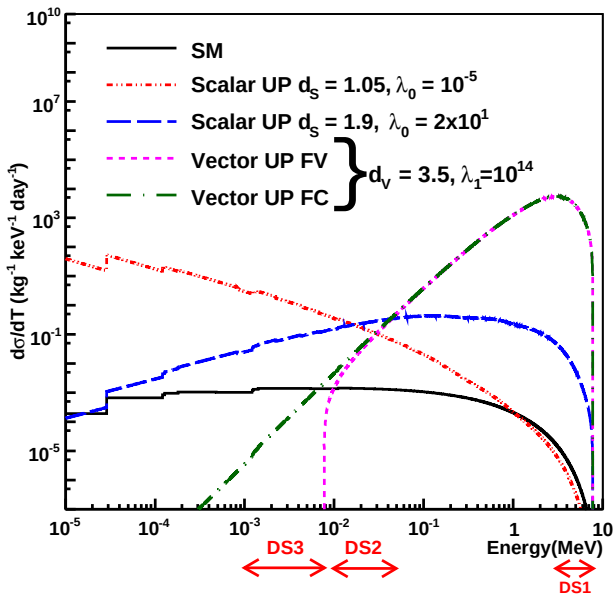

Figure 4.5: Differential cross-section as function of the recoil energy T with typical reactor-$\bar{\nu}_e$ spectra. Scalar UP, at two values of $(d_{\mathcal{S}}, \lambda_0)$ and vector UP, at a value of $(d_{\mathcal{V}}, \lambda_1)$ for both FV and FC cases, using Ge as target. The SM contributions are also superimposed. The relevant energy ranges of the three data sets used in the present analysis are also shown.

ticle exchange(Eq. 3.12) to the SM cross section Eq. 3.2 and find the event rate using Eq. 4.1. We applied a χ^2_{min} test and put limits on the parameter λ_0 (for scalar unparticle) and λ_1 (for vector unparticle) for various mass dimension $d_{\mathcal{S}}$ and $d_{\mathcal{V}}$ taking the unparticle energy scale, $\Lambda_{\mathcal{U}}$ = 1 TeV. To find the upper bounds for the coupling constants λ_0 and λ_1 at 90% C.L, after applying a fitting to λ_0^4 and λ_1^4 we again used the method explained in [107]. The results for the scalar unparticle case are shown in Figure 4.6. The bounds from the Borexino [111] and MUNU [104] experiments are superimposed to compare our results with the present ones. To understand the effect of unparticle energy scale $\Lambda_{\mathcal{U}}$, we placed upper bounds for some mass dimension parameter $d_{\mathcal{S}}$, $d_{\mathcal{S}}$ = 1.01, 1.4, 1.9 and varying the energy range $\Lambda_{\mathcal{U}}$ up to 10 TeV. These results are shown in Figure 4.7. Since MUNU and Borexino did not publish results for varying $\Lambda_{\mathcal{U}}$, we only showed our results with three different data sets.

The sensitivity of each experiment to the unparticle differs according to the mass dimension parameter $d_{\mathcal{S}}$. Therefore, as it is seen from Figures 4.6 and 4.7, for $d_{\mathcal{S}} < 1.3$ DS2-HPGe data gives more robust results and for $d_{\mathcal{S}} > 1.3$ DS1-CsI(Tl) data set has better sensitivity. Unparticle effects decrease as the energy scale $\Lambda_{\mathcal{U}}$ increases as shown in Figure 4.7.

Similarly, we perform the minimum χ^2 analysis method for the vector unparticle. We analyzed for both flavor conserving (FC) and flavor violating (FV) cases since the interference

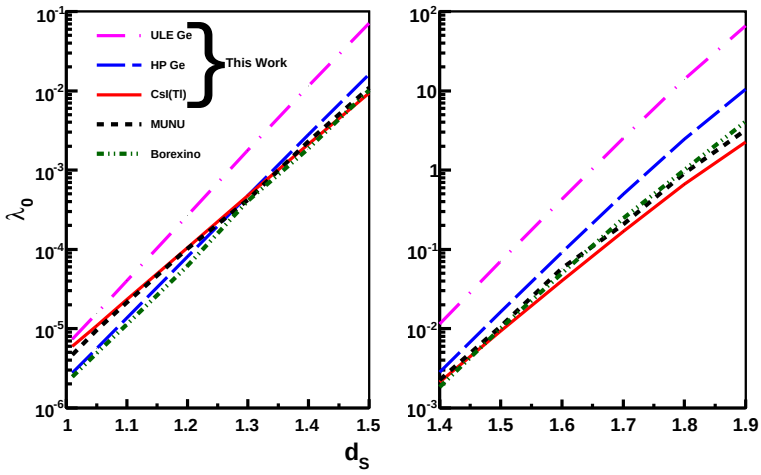

Figure 4.6: Constraints on UP with scalar exchange. The coupling λ_0 versus mass dimension d_S at Λ_U = 1 TeV are shown; Parameter space above the lines is excluded.

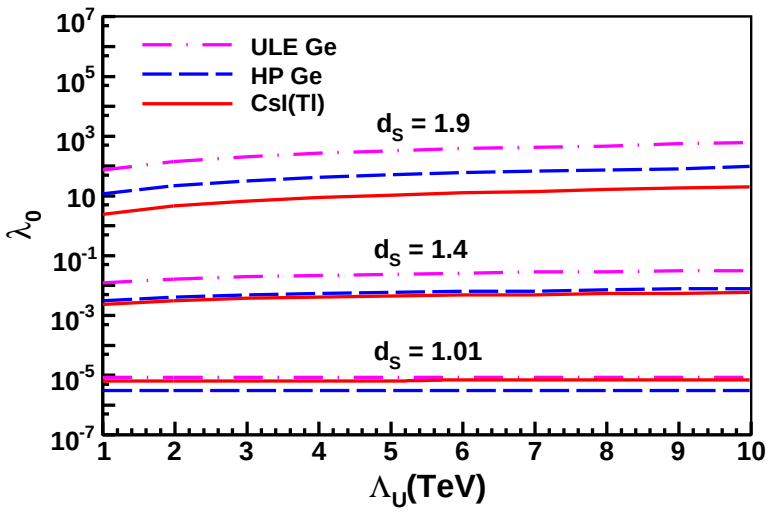

Figure 4.7: Constraints on UP with scalar exchange. Upper bounds on λ_0 at different energy scales Λ_U are displayed. Parameter space above the lines is excluded.

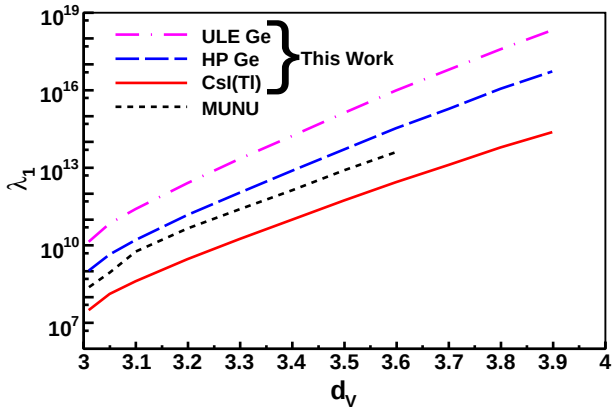

Figure 4.8: Constraints on UP with vector unparticle exchange – The coupling λ_1 versus $d_{\mathcal{V}}$ at $\Lambda_{\mathcal{U}} = 1$ TeV. The bounds apply for both FV and FC cases.

between SM and Unparticle can not be neglected for the flavor conserving case. Constraints on vector Unparticle couplings λ_1 vs some $d_{\mathcal{V}}$ parameters are shown in Figure 4.8. For this case both FC and FV couplings give similar bounds. The variations of λ_1 for both FV and FC cases as function of the energy $\Lambda_{\mathcal{U}}$ are shown in Figure 4.9. As d increases, the sensitivity of lower energy experiments decrease. Therefore, for vector unparticle case, Ds1-CsI(Tl) data set has better sensitivity. However, since there is theoretical bound on $d_{\mathcal{V}}$ as $d_{\mathcal{V}} > 3$, and vector unparticle effects become so small as d gets larger, the coupling constant bounds on λ_1 are too big. This result shows that $\bar{\nu}_e - e^-$ scattering experiment is not sensitive to vector unparticle parameters.

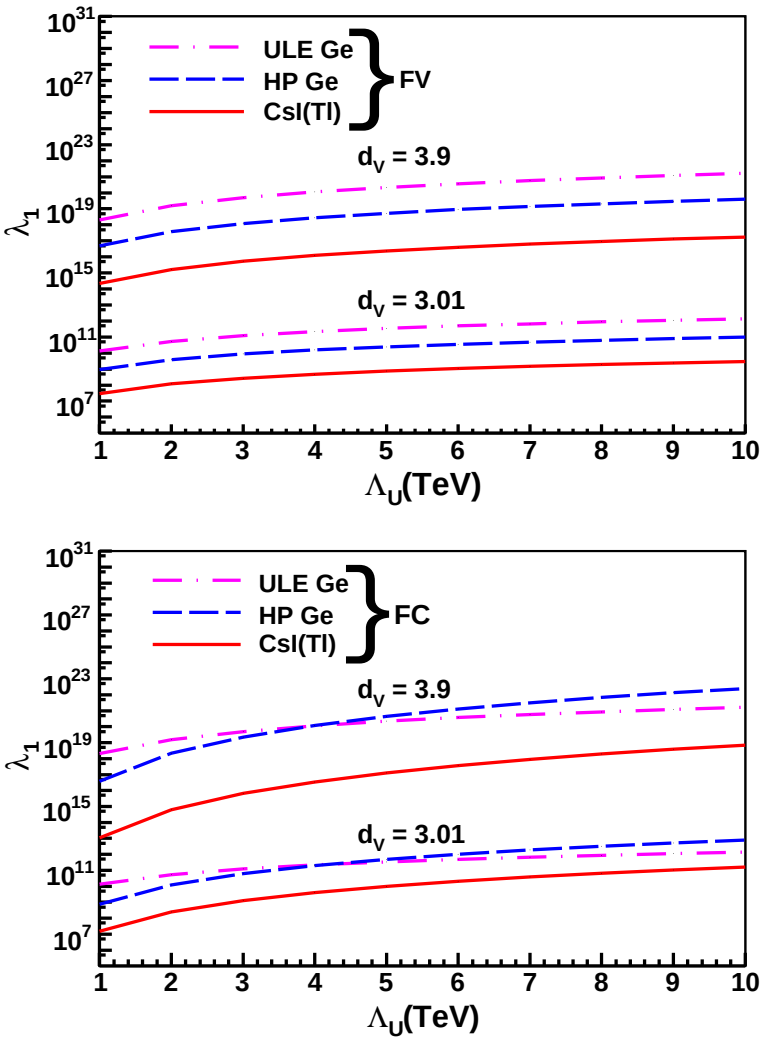

Figure 4.9: Constraints on UP with vector UP exchange. Upper bounds on λ_1 at different energy scales $\Lambda_{\mathcal{U}}$ for FV and FC couplings, respectively, at two values of $d_{\mathcal{V}}$. Parameter space above the lines is excluded.

REFERENCES

[1] http://lhc.web.cern.ch/lhc/ 13/09/2010

[2] H. T. Wong, H. B. Li, J. Li, Q. Yue and Z. Y. Zhou, J. Phys. Conf. Ser. **39**, 266 (2006) [arXiv:hep-ex/0511001].

[3] K. Scholberg, Phys. Rev. D **73**, 033005 (2006) [arXiv:hep-ex/0511042].

[4] P. Barbeau, J. I. Collar, J. Miyamoto and I. Shipsey, IEEE Trans. Nucl. Sci. **50**, 1285 (2003) [arXiv:hep-ex/0212034].

[5] R. Bernabei et al., Phys. Lett.B **480**, 23 (2000), and references therein.

[6] S. T. Lin et al., Phys. Rev. **D 79**, 061101(R) (2009).

[7] B. Kayser, Phys. Lett. **B 667**, 163 (2008), and references therein.

[8] P. S. Amanik, G. M. Fuller and B. Grinstein, Astropart. Phys. **24**, 160 (2005) [arXiv:hep-ph/0407130].

[9] T. Banks and A. Zaks, "On the phase structure of vector - like gauge theories with massless fermions," *Nucl. Phys.* **B196** (1982) 189.

[10] H. Georgi, Phys. Rev. Lett. **98**, 221601 (2007).

[11] H. Georgi, Phys. Lett. B **650**, 275 (2007).

[12] J. Chadwick, Verh. d. deutschen Phys. Ges. 16 (1914) 383.

[13] http://encyclopedia2.thefreedictionary.com/Negative+beta+decay 10/09/2010

[14] C. D. Ellis, Proc. Roy. Soc. (A), 101 (1922) 1.

[15] C.D. Ellis and W. A. Wooster, Proc. Roy. Soc. (A), 117, 109 (1927)

[16] L. Meitner and W. Orthmann, Z. Physik. 60 (1930) 143

[17] A. de Gouvea, arXiv:hep-ph/0411274.

[18] E. Rutherford, Phil. Mag, 1911, 21, ser.6, 669; ibid. 1912, 24, ser.6, 453

[19] R. Kronig, Naturw. 16 (1928) 335

[20] W. Heitler and G. Herzberg, Naturw. 17 (1929) 673

[21] From Albert Einstein: Philosopher-Scientist (1949), pub. Cambridge University Press, 1949. Neils Bohr's report of conversations with Einstein and Einstein's reply.

[22] Klaus Winter "Neutrino Physics" Cambridge University Press, (2008)

[23] http://web.lemoyne.edu/ giunta/ruth1920.html 07/09/2010

[24] Emilio Segre "From X-rays to Quarks: Modern Physicists and Their Discoveries, " Dover Publications (2007)

[25] http://www.kutl.kyushu-u.ac.jp/seminar/MicroWorld3_E/3Part1_E/3P13_E/DiscoverNeutron_E.htm 25/09/2010

[26] Nature 129, 312 (27 February 1932)

[27] E. Fermi, Ricercha Scient. 2 (1933) 12.

[28] E. Fermi, Z Physik. 88 (1934) 161.

[29] G.W Rodeback and J. S. Allen, Phys. Rev. 86 (1952) 446.

[30] Nickolas Solomey "The Elusive Neutrino: A Subatomic Detective Story " W.H. Freeman & Company; 1st edition, (1997)

[31] "Los Alamos Science", Number 25, (1997)

[32] Reines F and Cowan C L Jr, 1956, Nature 178 446, 523

[33] R. Davis, Phys. Rev. 97 (1955) 766.

[34] Kai Zuber, "Neutrino Physics," Series in High Energy Physics, Cosmology and Gravitation IoP Publising (2004)

[35] J. C. Street and E. C. Stevenson, Phys. Rev. 52, 1003â1004 (1937)

[36] Pontecorvo B 1960 Sov. J. Phys. 10 1256

[37] Danby G et al 1962 Phys. Rev. Lett. 9 36

[38] S. Eidelman et al. [Particle Data Group Colloboration, Phys. Lett. B 592,1 (2004)

[39] David Griffiths "Introduction to Elementary Particles," Wiley-VCH (2008)

[40] Groom D et al 2000 Review of particle properties. Eur. Phys. J .C **3** 1

[41] M. L. Perl,

[42] D. Abbaneo et.al hep-ex/0312023

[43] http://www.nu.to.infn.it/Fourth_Generation/ 07/09/2010

[44] http://dorigo.wordpress.com/2008/03/ 07/09/2010

[45] J.N. Bahcall, "Neutrino Astrophysics," Cambridge, Cambridge University Press (1989).

[46] von Weizsacker C F 1937 Z. Phys 38 176

[47] Bethe H A 1939 Phys. Rev. 55 434

[48] Rolfs C E and Rodney W S 1988 "Cauldrons in the Cosmos (University of Chicago Press)"

[49] J.N. Bahcall and M.H.Pinseaunault, Phys.Rev.Lett.92,121301 (2004) and references therein.

[50] Kuzmin V A 1966 Sov.Phys. JETP 22 1050

[51] Bahcall J N, Pinseaunault M.H and Basu S. 2001 Astrophys. J. 550 990

[52] Couvidat S, Turck-Chieze S and Kosovichev A G 2002 astro-ph/0203107

[53] Q. R. Ahmad et al. [SNO Collaboration] Phys. Rev. Lett. 89, 011301 (2002)

[54] E. Kearns, Nucl. Phys. Proc. Suppl. **70**, 315 (1999).

[55] Y.Fukuda et al.[Kamiokande Collaboration],Phys.Lett.B 237 (1994)

[56] Y.Fukuda et al.[Super-Kamiokande Collaboration], Phys. Rev. Lett. 81, 1562 (1998)

[57] B. Kayser, In the Proceedings of 32nd SLAC Summer Institute on Particle Physics (SSI 2004): Natures Greatest Puzzles, Menlo Park, California, 2-13 Aug 2004, pp L004 [arXiv:hep-ph/0506165].

[58] A. Strumia, Nucl. Phys. Proc. Suppl. **143** (2005) 144 [arXiv:hep-ph/0407132].

[59] http://hepmail.phys.sinica.edu.tw/ texono/

[60] M. Deniz *et al.* [TEXONO Collaboration], Phys. Rev. D **82** (2010) 033004 [arXiv:1006.1947 [hep-ph]].

[61] M. Deniz *et al.* [TEXONO Collaboration], Phys. Rev. D **81** (2010) 072001 [arXiv:0911.1597 [hep-ex]].

[62] H. B. Li et al., Phys. Rev. Lett. **90**, 131802 (2003); H. T. Wong et al., Phys. Rev. D **75**, 012001 (2007).

[63] H. M. Chang and H. T. Wong [TEXONO Collaboration], PoS **IDM2008** (2008) 103.

[64] H.T. Wong et al, J. Phys. Conf. Ser. **39**, 266 (2006).

[65] J. Erler and P. Langacker, Phys. Lett. **B 667**, 125 (2008), and references therein.

[66] L. Wolfenstein, Phys. Rev. **D 17**, 2369 (1978); J.W.F. Valle, Phys. Lett. **B 199**, 432 (1987); E. Roulet, Phys. Rev. **D 44**, 935 (1991); M.M. Guzzo, A. Masiero and S.T. Petcov, Phys. Lett. **B 260**, 154 (1991).

[67] K. Eguchi *et al.* [KamLAND Collaboration], Phys. Rev. Lett. **90** (2003) 021802 [arXiv:hep-ex/0212021].

[68] J. Schechter and J. W. F. Valle, Phys. Rev. **D 22**, 2227 (1980); A. Zee, Phys. Lett. **B 93**, 389 (1980); L. J. Hall, V. A. Kostelecky and S. Raby, Nuclear Physics **B 267**, 415 (1986); K. S. Babu, Phys. Lett. **B 203**, 132 (1988); M. Hirsch and J. W. F. Valle, New J. Phys. **6**, 76 (2004).

[69] T. Ohlsson and H. Zhang, Phys. Lett. B **671** (2009) 99 [arXiv:0809.4835 [hep-ph]].

[70] S. Bergmann, M. M. Guzzo, P. C. de Holanda, P. I. Krastev and H. Nunokawa, Phys. Rev. D **62** (2000) 073001 [arXiv:hep-ph/0004049].

[71] Z. Berezhiani, R. S. Raghavan and A. Rossi, Nucl. Phys. B **638** (2002) 62 [arXiv:hep-ph/0111138].

[72] A. Friedland, C. Lunardini and C. Pena-Garay, Phys. Lett. B **594** (2004) 347 [arXiv:hep-ph/0402266].

[73] O. G. Miranda, M. A. Tortola and J. W. F. Valle, JHEP **0610** (2006) 008 [arXiv:hep-ph/0406280].

[74] A. Bolanos, O. G. Miranda, A. Palazzo, M. A. Tortola and J. W. F. Valle, Phys. Rev. D **79** (2009) 113012 [arXiv:0812.4417 [hep-ph]].

[75] M. C. Gonzalez-Garcia *et al.*, Phys. Rev. Lett. **82** (1999) 3202 [arXiv:hep-ph/9809531].

[76] S. Bergmann, Y. Grossman and D. M. Pierce, Phys. Rev. D **61** (2000) 053005 [arXiv:hep-ph/9909390].

[77] N. Fornengo, M. Maltoni, R. Tomas and J. W. F. Valle, Phys. Rev. D **65** (2002) 013010 [arXiv:hep-ph/0108043].

[78] M. C. Gonzalez-Garcia and M. Maltoni, Phys. Rev. D **70** (2004) 033010 [arXiv:hep-ph/0404085].

[79] A. Friedland, C. Lunardini and M. Maltoni, Phys. Rev. D **70** (2004) 111301 [arXiv:hep-ph/0408264].

[80] A. Friedland and C. Lunardini, Phys. Rev. D **72** (2005) 053009 [arXiv:hep-ph/0506143].

[81] G. L. Fogli, E. Lisi, A. Mirizzi and D. Montanino, Phys. Rev. D **66** (2002) 013009 [arXiv:hep-ph/0202269].

[82] A. Esteban-Pretel, R. Tomas and J. W. F. Valle, Phys. Rev. D **76** (2007) 053001 [arXiv:0704.0032 [hep-ph]].

[83] J. Barranco, O. G. Miranda, C. A. Moura and J. W. F. Valle, Phys. Rev. D **73** (2006) 113001 [arXiv:hep-ph/0512195].

[84] J. Barranco, O. G. Miranda and T. I. Rashba, Phys. Rev. D **76** (2007) 073008 [arXiv:hep-ph/0702175].

[85] J. Barranco, O. G. Miranda and T. I. Rashba, JHEP **0512** (2005) 021 [arXiv:hep-ph/0508299].

[86] Z. Berezhiani and A. Rossi, Phys. Lett. B **535** (2002) 207 [arXiv:hep-ph/0111137].

[87] E. Roulet, Phys. Rev. D **44**, R935-938 (1991)

[88] A. De Gouvea, G. F. Giudice, A. Strumia and K. Tobe, Nucl. Phys. B **623** (2002) 395 [arXiv:hep-ph/0107156].

[89] T. Ota and J. Sato, Phys. Rev. D **71** (2005) 096004 [arXiv:hep-ph/0502124].

[90] M. Honda, Y. Kao, N. Okamura, A. Pronin and T. Takeuchi, arXiv:0704.0369 [hep-ph].

[91] M. Honda, Y. Kao, N. Okamura, A. Pronin and T. Takeuchi, arXiv:0707.4545 [hep-ph].

[92] M. B. Gavela, D. Hernandez, T. Ota and W. Winter, Phys. Rev. D **79** (2009) 013007 [arXiv:0809.3451 [hep-ph]].

[93] S. Antusch, J. P. Baumann and E. Fernandez-Martinez, Nucl. Phys. B **810** (2009) 369 [arXiv:0807.1003 [hep-ph]].

[94] M. Malinsky, T. Ohlsson and H. Zhang, Phys. Rev. D **79** (2009) 011301 [arXiv:0811.3346 [hep-ph]].

[95] Y. Grossman, Phys. Lett. B **359** (1995) 141 [arXiv:hep-ph/9507344].

[96] S. Bergmann, Y. Grossman and E. Nardi, Phys. Rev. D **60** (1999) 093008 [arXiv:hep-ph/9903517].

[97] M. Blennow, T. Ohlsson and W. Winter, Eur. Phys. J. C **49** (2007) 1023 [arXiv:hep-ph/0508175].

[98] A. de Gouvea and J. Jenkins, Phys. Rev. D **77** (2008) 013008 [arXiv:0708.1344 [hep-ph]].

[99] S. Davidson et al., JHEP **0303**, 011 (2003).

[100] J. Barranco et al., Phys. Rev. **D 73**, 113001 (2006); J. Barranco et al., Phys. Rev. **D 77**, 093014 (2008).

[101] K. Cheung, W.Y. Keung and T.C. Yuan, Phys. Rev. Lett **99**, 051803 (2007); K. Cheung, W.Y. Keung and T.C. Yuan, Phys. Rev. **D 76**, 055003 (2007).

[102] S. L. Chen and X. G. He, Phys. Rev. **D 76**, 091702 (2007).

[103] A. B. Balantekin and K. O. Ozansoy, Phys. Rev. **D 76**, 095014 (2007).

[104] J. Barranco et al., Phys. Rev. **D 79**, 073011 (2009).

[105] A. M. Green, Phys. Rev. D **65** (2002) 023520 [arXiv:astro-ph/0106555].

[106] C. Savage et al., JCAP **04**, 010, Section 3.2 (2009).

[107] G. J. Feldman and R. D. Cousins, Phys. Rev. D 57, 3873 (1998).

[108] C. Biggio, M. Blennow and E. Fernandez-Martinez, JHEP **0903**, 139 (2009); C. Biggio, M. Blennow and E. Fernandez-Martinez, JHEP **0908**, 090 (2009).

[109] S. Zhou, Phys. Lett. B **659** (2008) 336 [arXiv:0706.0302 [hep-ph]].

[110] B. Grinstein, K. A. Intriligator and I. Z. Rothstein, Phys. Lett. B **662** (2008) 367 [arXiv:0801.1140 [hep-ph]].

[111] D. Montanino, M. Picariello and J. Pulido, Phys. Rev. D **77** (2008) 093011 [arXiv:0801.2643 [hep-ph]].

[112] S.A. Fayans, L.A. Mikaelyan and V.V. Sinev, Phys. Atom. Nucl. **64**, 1475 (2001); H.T. Wong, H.B. Li and S.T. Lin, Phys. Rev. Lett., **105**, 061801 (2010).